Biomaterial Microstructure and Properties: The Relevance of Biomimetics and Bioengineering

Expert Insights

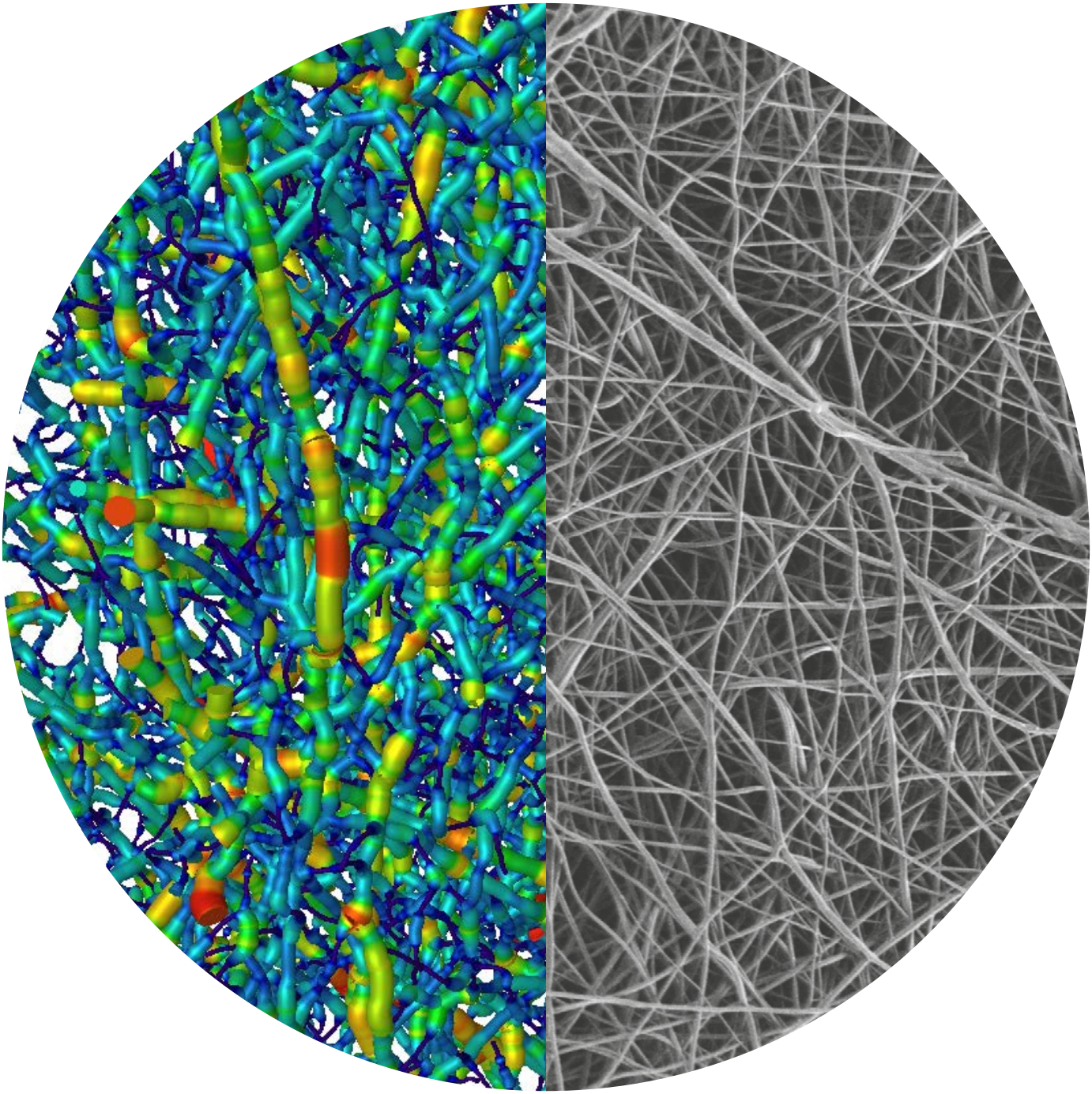

ZEISS

Seeing beyond

WILEY

Synchrotron-quality nanoscale 3D X-ray imaging in your lab

ZEISS Xradia 810 Ultra

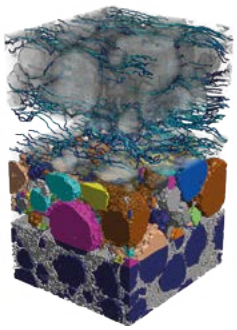

Experience performance and flexibility using non-destructive nanoscale 3D imaging. Unique synchrotron-quality optics achieve spatial resolution down to 50 nm with absorption and phase contrast. Maximize contrast and throughput with the system optimized for 5.4 keV X-ray energy. Leverage unique *in situ* 3D imaging capabilities to study structural evolution over time and under varying conditions.

zeiss.com/810ultra

ZEISS

Seeing beyond

Contents

BACK TO CONTENTS

Editorial

Biomimetic engineering blends nature's inspiration – spider silk, lotus leaves, bamboo – to create sustainable materials through interdisciplinary collaboration in science and engineering. These materials are now a noteworthy alternative to traditional natural or synthetic materials, finding applications not only in regenerative medicine but also in renewable energy devices and sensor technology. Understanding the interplay between processing, properties, and structural influences is essential for designing tomorrow's biomimetic materials, and characterization plays a crucial role in perfecting their performance across scales. Therefore, comprehensive characterization of biomaterial structures, from macro to nanoscales, using advanced techniques, is vital for successful bio-structure research and engineering.

The first article within this compendium by Lizundia and coworkers explores the use of biodegradable cellulose nanoparticles to create a gel polymer electrolyte for sustainable energy storage beyond lithium-ion batteries [1]. Next, Liu *et al*. employ thermal scanning probe lithography to achieve cost-effective, high-throughput fabrication of large-area quasi-3D bone tissue replicas with exceptional precision [2]. Then, Zhao *et al*. demonstrate a room-temperature process combining localized mineralization and emulsion-based 3D printing to create centimeter-sized biominerals [3].

Mao *et al*. introduce bioinspired 3D printing as a key approach for designing mechanically efficient cellular materials essential for aerospace, lightweight vehicles, and energy absorption applications [4].Then, Lenges and coworkers report the enzymatic polymerization of sucrose into engineered polysaccharides, particularly alpha-1,3 glucan, as a sustainable performance additive for thermoplastic polyurethane materials [5]. And lastly, Qing *et al*. utilize the unique hierarchical microstructures of the *Morpho* butterfly wing, by depositing an azobenzene-containing linear liquid crystal polymer on the template to create a photonic crystal with potential applications in pigments, cosmetics, and sensors [6].

To gain insights into the exciting realm of nature-inspired materials, we had the privilege of interviewing Associate Professor Erlantz Lizundia, coauthor of the first article in this compendium. This interview delves into Professor Lizundia's extensive expertise in the field, highlighting the current trends and essential takeaways that resonate throughout this eBook.

Through the methods and applications presented in this expert insight, we hope to educate researchers on new technologies and techniques for the characterization of biomaterials. For more information, we encourage you to visit ZEISS to learn more and explore options to enhance your research.

Christene A. Smith, Ph.D.
Editor at Wiley

References

[1] Mittal, N. et al. (2022). Hierarchical Nanocellulose-Based Gel Polymer Electrolytes for Stable Na Electrodeposition in Sodium Ion Batteries. *Small*. DOI: 10.1002/smll.202107183.

[2] Liu, X. et al. (2021). Cost and Time Effective Lithography of Reusable Millimeter Size Bone Tissue Replicas With Sub-15 nm Feature Size on A Biocompatible Polymer. *Advanced Functional Materials*. DOI: 10.1002/adfm.202008662.

[3] Zhao, R. et al. (2023). Additive Manufacturing of Porous Biominerals. *Advanced Functional Materials*. DOI: 10.1002/adfm.202300950.

[4] Mao, A. et al. (2021). Mechanically Efficient Cellular Materials Inspired by Cuttlebone. *Advanced Materials*. DOI: 10.1002/adma.202007348.

[5] Mok, J.W. et al. (2021). Evaluation of the engineered polysaccharide alpha-1,3 glucan in a thermoplastic polyurethane model system. *Journal of Applied Polymer Science*. DOI: 10.1002/app.49931.

[6] Qing, X. et al. (2019). Phototunable *Morpho* Butterfly Microstructures Modified by Liquid Crystal Polymers. *Advanced Optical Materials*. DOI: 10.1002/adom.201801494.

BACK TO CONTENTS

Biomaterial Microstructure and Properties

The Relevance of Biomimetics and Biomaterials Today

The flexibility and strength of spider silk, the self-cleaning capability of lotus leaves, and the strength of bamboo are only some examples that nature already has the answers to many of the problems we face today, such as creating new materials from renewable sources with properties like durability or sustainability. Designing materials inspired by nature is the basic idea of biomimetic and biomaterials engineering. This rapidly developing interdisciplinary field closely combines very different research areas such as materials science and biology, chemistry and physics, or mechanical engineering and medicine.

As demonstrated by the aforementioned examples, in terms of sustainability, biomaterials science can meet multiple needs while aiming for a dynamic balance with the ecosystem of our planet. The inspiration for new bio-fabrication methods comes from shapes in nature. Resulting new bio-inspired materials show outstanding performance and are used for tissue engineering and regeneration, bone reconstruction, biocompatible implants, sensors, or even new materials for sustainable energy devices - making it relevant for all of us.

However, all these efforts will not be successful until the properties of the materials are understood in detail. Therefore, it is vital to examine the structure-property-process relationship of biomaterials in detail and characterize their structures comprehensively from the macro- to the micro- and nanoscale. Measuring and mimicking structures may seem to be straightforward at first glance, however, experimental conditions can be very challenging hence every improvement of structural characterization is most valuable. Multi-modal microscopic imaging and analytical techniques are used to correlate results from several modalities and over different length scales to provide maximum insight. Ranging from surface characterization to 3D computed tomography or computational simulation of models, each technique is crucial for the research and engineering of bio-structures (Fig. 1).

What Are the Aims and Scope of Biomaterials Research?

Where conventional natural biomaterial or merely synthetic material was used in the past, nowadays biomimetic materials have become a remarkable alternative. Use cases are not only found in regenerative medicine but also in renewable energy devices and sensor technologies.

The use of biodegradable cellulose nanoparticles for the preparation of a gel polymer electrolyte may open new opportunities for sustainable energy storage systems as a resource [1]. In this case, testing of electrical properties can be related to the microstructure revealed with a scanning electron microscope (SEM).

Bio-inspired materials such as mimetic scaffolds mimic the *in vivo* environment and possess mechanical adaptability, microstructural interconnectivity, and inherent bioactivity, making them ideal for implants and regenerative medicine. When creating biomimetic surfaces for bone tissue replicas e.g., with thermal scanning probe lithography, it is essential to control surface quality. The techniques of choice for this application are high-resolution imaging and measurements in an SEM combined with confocal laser scanning microscopy (LSM) [2]. In addition to the surface roughness properties of the sample, the LSM reveals the biocompatibility by fluorescence imaging of the appropriate staining of the cells attached to the surface. The cell morphology is examined via low-voltage FE-SEM imaging (FE for field emission).

An X-ray microscope (XRM) or µ-CT (micro-computed tomography) is used to image biomaterials and bio-inspired 3D printed materials [3,4]. Controlled adjustment of microstructural properties such as porosity [3] is key to understanding the biomineralized materials. The 3D data obtained with this technique can be used as a high-quality model for a 3D printed structure for applications such as locomotive applications, aerospace structures, or implantable devices.

Foams made of polymer blends like polyurethanes with additives are essential in modern technologies, but achieving renewable, performant, cost-effective building blocks under scalable production conditions is a challenge. Polysaccharides are renewable materials as they can be produced from glucan by enzymatic polymerization and are suitable additives. The three-dimensional structure is one key aspect of the performance of the foam. Investigations with SEM and XRM help to understand its mechanical properties and porosity [5]. The discovery of a biocompatible polysaccharide as an additive from a renewable source might lead to a novel scalable process technology.

The link between microstructure and optical properties with potential applications in pigments, cosmetics, and sensors can be examined with FE-SEM technology [6]. Here, a phototunable structure has been fabricated by depositing the azobenzene-containing linear liquid crystal polymer (LLCP) onto the *Morpho* butterfly wing (MBW) used as a template. Instead of fully

Figure 1

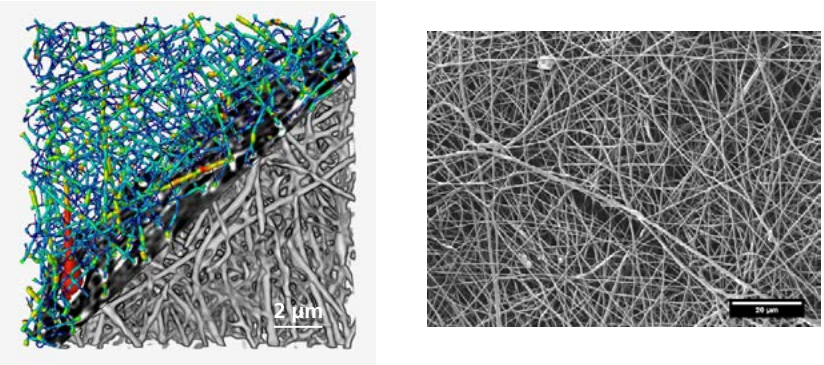

Fig. 1: *Characterization of the 3D microstructure of gelatin fibres for nanofibrous scaffolds for tissue engineering. (Right: XRM dataset acquired with ZEISS Xradia Ultra, left: SEM image acquired with a ZEISS FE-SEM).*

Figure 2

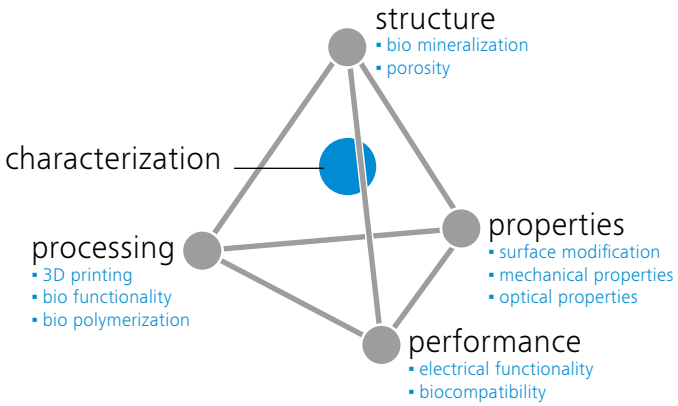

Fig. 2: *The cornerstones of the materials design paradigm with characterization as the key. Solving the challenge of connecting processing and structure with properties and performance is a key requirement for materials engineering.*

reconstructing the structures, modifying MBW with responsive coatings retains its delicate microstructures and optical properties while allowing tunable reflection to external stimuli. FE-SEM was applied to investigate the topological change of the samples during the fabrication process.

Microscopy Essentials for Biomaterials Research

Designing tomorrow's biomimetic materials needs an understanding of the connection between processing, properties, and the structures that influence how a material performs and why it might fail. Characterization is the key (Fig. 2) that enables researchers to connect these dots and optimize a material's performance. The investigation of its structure from the millimeter to the nanometer scale requires more than just one microscopic modality. Analytics are essential not only for investigation but also for improving the properties.

For many of these use cases, multi-modal, multi-scale microscopy delivers valuable insights linking information over length scales and correlating images with analytical data by combining light-, X-ray-, and electron microscopy enabled by sophisticated yet easy-to-use software.

When bioengineers or researchers need multi-scale information ranging from the millimeter to the sub-micrometer scale, X-ray microscopes are ideally suited. Non-destructive 3D X-ray imaging supports exceptional visualization and structure contrast enabling the investigation of large sample volumes with overview scans, allowing the researcher to keep the sample intact at the same time. Detailed XRM scans at higher magnifications deliver resolution in the range of sub-microns or even a few hundred nanometers depending on application requirements and instrument class. The 3D datasets generated use interactive virtual cross-sections that can be viewed from any orientation. Users obtain data in a matter of hours and virtual 2D cross-sections at any location or orientation required. Resolution-at-a-Distance (RaaD) is the two-stage magnification technique that unlocks high resolution and helps to provide the information needed for accurate localization of every microstructural detail. Soft materials experiments especially benefit from the different XRM imaging contrasts such as absorption or propagation phase contrast. For enhanced absorption contrast, highly specialized proprietary detectors are optimized to maximize the collection of contrast-forming low-energy X-ray photons. The tunable phase contrast modality measures the refraction of X-rays and enables visualization of materials with poor absorption contrast such as polymers or other low Z materials. All these data can be correlated with sample preparation techniques, such as FIB-SEM, and guide decisions for the next experimental steps, for example, such as destructive physical analysis.

When it comes to gaining speed, improving image quality, or when users need to upscale data for detailed reconstructions, artificial intelligence (AI)-powered tomography reconstruction techniques are now being used. One can improve scan throughput by 4x – 10x. Alternatively, it is possible to make reconstructions faster up to a factor of 100 by using high-resolution 3D microscopy datasets as training data for lower resolution, larger field-of-view datasets, and upscale the larger volume data using a neural network model. 3D XRM is the ideal instrument to visualize microstructural details and key structures within intact samples in a non-destructive manner making it the natural starting point for a multi-modal experiment.

Figure 3

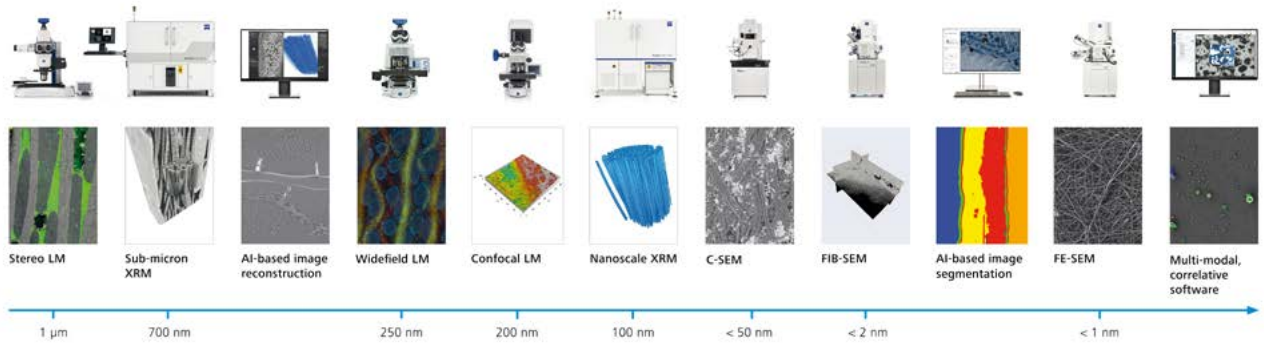

Fig. 3: *A synergistic portfolio for imaging across scales - light-, X-ray- and electron microscopes (LM, XRM, EM), supported by correlative image analysis software enables a comprehensive characterization of biomaterials.*

Biomaterials are often low-density, non-conducting, maybe outgassing organic samples. When investigated with scanning electron microscopes, these specimens react to the vacuum conditions by charging and to the interactions with the scanning electron beam by impeding good image quality. To achieve surface-sensitive, high-resolution information with sharp contrast, minimized charging effects and beam damage, researchers need a field emission SEM with advanced electron optics and sophisticated low vacuum technology. For example, the Gemini electron optics in FE-SEMs from ZEISS are tailored to high-resolution, low-voltage imaging with excellent contrast. For the most sensitive samples, the experiments can be run under environmental conditions known as Nano-VP which has been designed to reduce the charging effect and deliver high resolution and sharp contrast at the same time. Furthermore, correlative XRM-SEM or focused ion beam scanning electron microscope (FIB-SEM) workflows steered by dedicated software tools, in a correlative ecosystem, accelerate the creation of meaningful results by connecting tools seamlessly and enabling researchers to quickly navigate between multiple length scales and imaging modes.

In the investigation of biomaterials, understanding the interaction between the inorganic and organic material e.g., an implant and the organic bone tissue, plays a crucial role in successful patient recovery. Typical tasks and applications in this context may be the investigation of cell growth and biofilms on surfaces and the analysis of surface roughness and topography. A research-grade light microscope combined with an LSM offers a unique combination for scientists to image the surface structure of an inorganic material while simultaneously imaging multi-stained cells with fluorescence. LSMs can strongly support the creation of innovative products based on biomimetic materials. One focus is on the microstructure, although the surface topography also has a major influence on material properties. In addition, novel production processes and design options are expanding all the time. Here, an LSM allows engineers to quickly assess their novel material with advanced light microscopic, even fluorescent imaging, and investigate and measure surface topography parameters at the same time.

For a wide range of applications, multi-modal, multi-scale microscopy delivers valuable insights into every detail of biomaterials setting a standard for the understanding of measured properties. All length scales from millimeters to nanometers can be investigated by using and combing light-, X-ray-, and electron microscopy and analytics (Fig. 3).

References

[1] Mittal, N. et al. (2022). Hierarchical Nanocellulose-Based Gel Polymer Electrolytes for Stable Na Electrodeposition in Sodium Ion Batteries. *Small*. DOI: 10.1002/smll.202107183.

[2] Liu, X. et al. (2021). Cost and Time Effective Lithography of Reusable Millimeter Size Bone Tissue Replicas With Sub-15 nm Feature Size on A Biocompatible Polymer. *Advanced Functional Materials*. DOI: 10.1002/adfm.202008662.

[3] Zhao, R. et al. (2023). Additive Manufacturing of Porous Biominerals. *Advanced Functional Materials*. DOI: 10.1002/adfm.202300950.

[4] Mao, A. et al. (2021). Mechanically Efficient Cellular Materials Inspired by Cuttlebone. *Advanced Materials*. DOI: 10.1002/adma.202007348.

[5] Mok, J.W. et al. (2021). Evaluation of the engineered polysaccharide alpha-1,3 glucan in a thermoplastic polyurethane model system. *Journal of Applied Polymer Science*. DOI: 10.1002/app.49931.

[6] Qing, X. et al. (2019). Phototunable *Morpho* Butterfly Microstructures Modified by Liquid Crystal Polymers. *Advanced Optical Materials*. DOI: 10.1002/adom.201801494.

Authors:

Dr. Markus Boese
Business Sector Manager Soft Materials
ZEISS Research Microscopy Solutions

Dr. Sabine Lenz
Marketing Specialist
ZEISS Research Microscopy Solutions

Hierarchical nanocellulose-based gel polymer electrolytes for stable Na electrodeposition in sodium-ion batteries

Adapted from Neeru Mittal, Sean Tien, Erlantz Lizundia *et al.* Article link

Sodium-ion batteries based on earth-abundant materials offer efficient, safe, and environmentally sustainable solutions for a decarbonized society. However, to compete with mature energy storage technologies such as lithium-ion batteries, further progress is needed, particularly regarding energy density and operational lifetime. Considering these aspects, the authors use biodegradable cellulose nanoparticles for the preparation of a gel polymer electrolyte that may open up new opportunities for sustainable energy storage systems beyond lithium-ion batteries. SEM analyses were performed on a DSM 982 Gemini (ZEISS).

Introduction

Rechargeable batteries are one of the cornerstones of the green energy transition and are destined to play a crucial role in the decarbonization and electrification of worldwide economies. Sodium-ion batteries (NIBs) are a viable alternative to the ubiquitous lithium-ion batteries (LIBs). NIBs show generally lower impacts in global warming, fossil depletion potential, freshwater eutrophication, and human toxicity potential when compared to LIBs [1]. However, the lower theoretical capacity of Na compared to Li limits the implementation of NIBs in large-scale stationary applications [1,2].

The separator–electrolyte pair is a critical component defining the electrochemical performance and battery safety [1,2]. Conventional NIBs use a petroleum-based polyolefin or a glass fiber separator soaked into an organic electrolyte [3]. However, this configuration suffers from inferior electrochemical performance and safety issues, in consequence, replacing it with a gel-like electrolyte represents a step forward toward safer batteries [4]. In this regard, polymers with polar functional groups play a predominant role, given their potential to dissolve alkali metal salts [5]. Due to their improved mechanical properties compared to traditional microporous separators, gel polymer electrolytes (GPEs) are particularly advantageous in suppressing the formation of high surface area metal deposits [4,5].

Biopolymers show functional properties equivalent to or above those of synthetic polymers, offering additional attractive features including renewability, biodegradability, and lack of toxicity [6,7]. Particularly relevant are biopolymer electrolytes based on cellulose [8,9], which offer environmentally sustainable and cost-effective alternatives to petroleum-based conventional choices. Following a circular "reuse, recycle or biodegradable" perspective, here we develop for the first time a biopolymer-based gel electrolyte for NIBs.

Results and Discussion

Fabrication and Morphology

As summarized in Scheme 1, cellulose nanocrystals (CNCs) and cellulose nanofibers (CNFs) are first extracted from lignocellulosic biomass [10]. Using a chemically induced hydrolysis or a mechanically induced destructuring approach assisted by TEMPO-mediated oxidation [11], the microfibrils that constitute the plant cell wall can be selectively broken down into colloidal building blocks to obtain spindle-shaped CNCs or filament-like CNFs [12]. During this process, the surface of CNCs is decorated with anionic sulfate half-ester groups ($–OSO_3^-$) [13], while negatively charged carboxyl groups carrying Na^+ as counterions ($–COO^-$) are present on CNFs [11]. Once the gel is formed, the aqueous gel phase can be easily replaced by a gas phase through freeze-drying, resulting in highly porous lightweight materials with a hierarchical porous structure and average pore size in the tens of nanometers. These cryogels can be applied as a matrix for the development of GPEs after the infusion of ionically conducting liquid electrolytes.

After the infusion of the liquid electrolyte, glutaraldehyde is added as a chemical cross-linker

Scheme 1

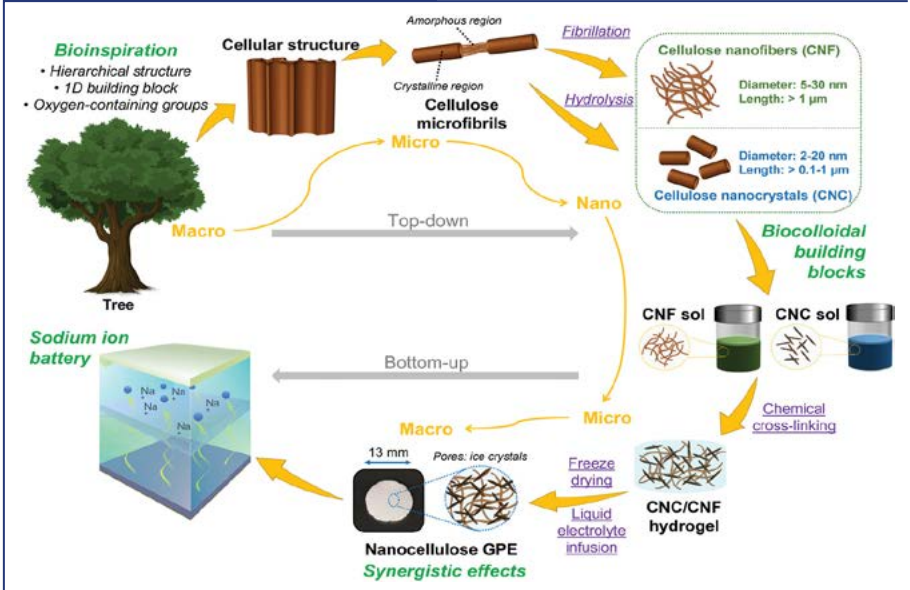

Scheme 1: *A top-down approach is followed to extract biocolloidal CNCs and CNFs from biomass, followed by bottom-up preparation of the CNC/CNF cryogel using a combination of self-assembly and sol-gel chemistry. GPEs are finally obtained upon organic liquid infiltration.*

to form acetal linkages between the hydroxyl groups of the nanocelluloses [14]. The incorporation of long and flexible CNFs provides physically entangled networks that facilitate hydrogel formation [15], which after glutaraldehyde crosslinking and freeze-drying result in macroscopic porous cryogels. These cryogels after the infusion of liquid electrolyte (1 m $NaClO_4$ in ethylene carbonate/propylene carbonate (EC/PC) at 50/50 v/v) yield physically stable GPEs. Figure 1 shows the top-view and cross-sectional scanning electron microscopy (SEM) images of CNC/CNF 80/20, 50/50, and 20/80 cryogels. Highly porous structures with isotropically distributed three-dimensionally connected pores are achieved for all the compositions, both at the surface and across the entire cryogel thickness. Therefore, the abundant –OH surface groups present in CNCs and CNFs will remain available to solvate Na^+ and to separate it from ClO_4^-, facilitating ion diffusion between electrodes [8]. Interestingly, the 50/50 freeze-dried cryogel shows a rough morphology, being composed of smaller and more abundant pores, which is desired for GPEs to obtain high ionic conductivity.

GPE Physico-Electrochemical Properties

Voltametric measurements (0.3–5 V) versus Na/Na^+ showed that the 50/50 GPE exhibited the best cathodic stability, outperforming

Figure 1

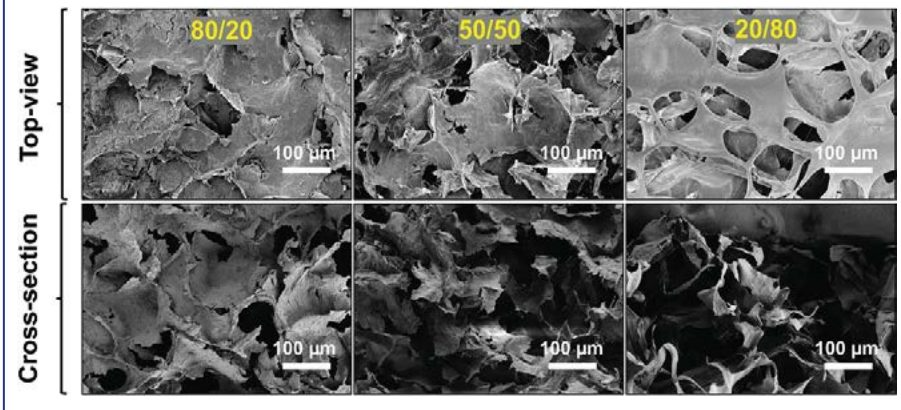

Fig. 1: *Representative SEM images showing the top-view and cross-section of CNC/CNF-based cryogels at 80/20, 50/50, and 20/80 ratios.*

Figure 2

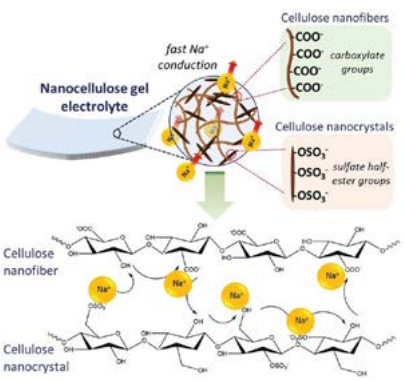

Fig. 2: *Schematic illustration of the proposed Na^+ conduction mechanism across the nanocellulose GPE.*

other GPEs based on thermoplastics [16]. Such large electrochemical stability enables the implementation of cathodes with higher voltages than the well-known $Na_3V_2(PO_4)_3$ with a working voltage window of 2.8–3.8V versus Na/Na^+. As schematized in Figure 2, the increased Na^+ conductivity and transference values of the nanocellulose GPE are achieved thanks to the synergistic effects of CNCs and CNFs, which combine –OH, $–OSO_3^-$, and $–COO^-$ groups.

Electrochemical Performance of GPEs

Sodium electrodeposition was assessed in symmetric Na/Na cells by successive plating and stripping cycles. The results indicate that the 50/50 formulation ensures an improved Na ion transference reversibility and homogeneous Na electrodeposition between electrodes. This performance represents a significant improvement over the Na plating and stripping results reported so far for symmetric Na/Na cells with separators soaked in a liquid electrolyte (Fig. 3)

Figure 3

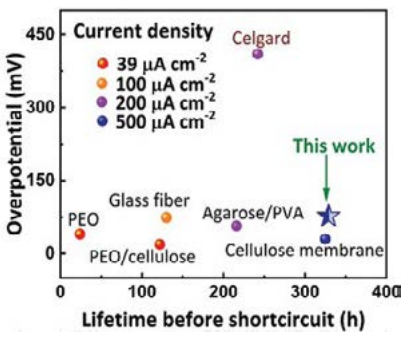

Fig. 3: *Comparison with the state-of-the-art separator–liquid electrolyte pairs.*

Battery Performance

The reversible capacity provided by the nanocellulose gel electrolyte in combination with the high working voltage of the battery result in a gravimetric energy density (based on the active mass of the cathode) of 240 Wh kg^{-1} at a rate of 1C, making this system competitive against current LIBs. It is important to note that the nanocellulose gel electrolyte here developed surpasses the specific capacities provided by other separator-liquid electrolyte systems with $Na_3V_2(PO_4)_3$ as the cathode [17–19].Yet, the developed nanocellulose gel electrolytes still have room to improve the electrochemical performance by reducing their thickness to 25–30 µm.

Conclusions

Biomass resources are used for the first time to synthesize a biopolymer-based gel electrolyte offering a good balance between the often mutually exclusive renewability and electrochemical performance. When assembled in $Na_2Fe_2(SO_4)_3$/Na half-cells, nanocellulose gel electrolytes present good capacity retention with a gravimetric energy density (based on cathode mass) of 240 Wh kg^{-1} at a rate of 1C, surpassing the electrochemical performance of the conventional separator-electrolyte pairs relying on fossil resources.

References

[1] Arora, P. and Zhang, Z. (2004). Battery separators. *Chemical Reviews*. DOI: 10.1021/CR020738U/ASSET/IMAGES/MEDIUM/CR020738UE00011.GIF.

[2] Zhang, B. et al. (2014). A superior thermostable and nonflammable composite membrane towards high power battery separator. *Nano Energy*. DOI: 10.1016/J.NANOEN.2014.10.001.

[3] Kundu, D. et al. (2015). The Emerging Chemistry of Sodium Ion Batteries for Electrochemical Energy Storage. *Angewandte Chemie International Edition*. DOI: 10.1002/ANIE.201410376.

[4] Ferrari, S. et al. (2021). Solid-State Post Li Metal Ion Batteries: A Sustainable Forthcoming Reality? *Advanced Energy Materials*. DOI: 10.1002/AENM.202100785.

[5] Xu, D. et al. (2018). High-Strength Internal Cross-Linking Bacterial Cellulose-Network-Based Gel Polymer Electrolyte for Dendrite-Suppressing and High-Rate Lithium Batteries. *ACS Applied Materials and Interfaces*. DOI: 10.1021/ACSAMI.8B00034/ASSET/IMAGES/LARGE/AM-2018-000349_0008.JPEG.

[6] Gandini, A. (2008). Polymers from renewable resources: A challenge for the future of macromolecular materials. *Macromolecules*. DOI: 10.1021/MA801735U/ASSET/IMAGES/MEDIUM/MA-2008-01735U_0002.GIF.

[7] Zhu, Y. et al. (2016). Sustainable polymers from renewable resources. *Nature 2016 540:7633*. DOI: 10.1038/nature21001.

[8] Qin, H. et al. (2020). Flexible nanocellulose enhanced Li+ conducting membrane for solid polymer electrolyte. Energy Storage Materials. DOI: 10.1016/J.ENSM.2020.03.019.

[9] Gou, J. et al. (2020). A renewable gel polymer electrolyte based on the different sized carboxylated cellulose with satisfactory comprehensive performance for rechargeable lithium ion battery. Polymer. DOI: 10.1016/J.POLYMER.2020.122943.

10 Li, T. et al. (2021). Developing fibrillated cellulose as a sustainable technological material. *Nature 2021 590:7844*. DOI: 10.1038/s41586-020-03167-7.

[11] Okita, Y. et al. (2010). Entire Surface Oxidation of Various Cellulose Microfibrils by TEMPO-Mediated Oxidation. Biomacromolecules. DOI: 10.1021/BM100214B.

[12] Heise, K. et al. (2021). Nanocellulose: Recent Fundamental Advances and Emerging Biological and Biomimicking Applications. *Advanced Materials*. DOI: 10.1002/ADMA.202004349.

[13] Hänsel, C. et al. (2019). A Single Li-Ion Conductor Based on Cellulose. ACS Applied *Energy Materials*. DOI: 10.1021/ACSAEM.9B00821/ASSET/IMAGES/LARGE/AE-2019-008216_0005.JPEG.

[14] Jeon, J.G. et al. (2019). Cross-linking of cellulose nanofiber films with glutaraldehyde for improved mechanical properties. *Materials Letters*. DOI: 10.1016/J.MATLET.2019.05.002.

[15] De France, K.J. et al. (2017). Review of Hydrogels and Aerogels Containing Nanocellulose. *Chemistry of Materials*. DOI: 10.1021/ACS.CHEMMATER.7B00531/ASSET/IMAGES/LARGE/CM-2017-00531A_0012.JPEG.

[16] Park, M.S. et al. (2019). Thermoplastic Polyurethane Elastomer-Based Gel Polymer Electrolytes for Sodium-Metal Cells with Enhanced Cycling Performance. *ChemSusChem*. DOI: 10.1002/CSSC.201901799.

[17] Zhang, J. et al. (2017). In Situ Formation of Polysulfonamide Supported Poly(ethylene glycol) Divinyl Ether Based Polymer Electrolyte toward Monolithic Sodium Ion Batteries. *Small*. DOI: 10.1002/SMLL.201601530.

[18] Zhang, T.W. et al. (2017). Prawn shell derived chitin nanofiber membranes as advanced sustainable separators for Li/Na-Ion Batteries. *Nano Letters*. DOI: 10.1021/ACS.NANOLETT.7B01875/ASSET/IMAGES/LARGE/NL-2017-018754_0005.JPEG.

[19] Ojanguren, A. et al. (2021). Stable Na Electrodeposition Enabled by Agarose-Based Water-Soluble Sodium Ion Battery Separators. ACS *Applied Materials and Interfaces*. DOI: 10.1021/ACSAMI.1C02135/ASSET/IMAGES/LARGE/AM1C02135_0006.JPEG.

BACK TO CONTENTS

Cost and time effective lithography of reusable millimeter size bone tissue replicas with sub-15 nm feature size on a biocompatible polymer

Adapted from Xiangyu Liu, Alessandra Zanut, Martina Sladkova-Faure, *et al.* Article link

Thermal scanning probe lithography (tSPL) is proposed for the low-cost and high-throughput nanofabrication of large-area quasi-3D bone tissue replicas with high fidelity, sub-15 nm lateral precision, and sub-2 nm vertical resolution. Fluorescence of the bone tissue topography pattern was measured using ZEISS LSM 880 Airyscan laser scanning confocal microscopy with excitation at 488 nm and emission detection range 510–600 nm. ImageJ was used to adjust optical contrast in fluorescent images. Confocal images of cells on the bone tissue replica were taken with a ZEISS Axiovert 200M light microscope and LSM 5 Pascal exciter and software (ZEISS) with defined settings. SEM imaging examined cell morphology on PMCC-coated ITO glass. Samples were fixed with 2.5% v/v glutaraldehyde in sodium cacodylate buffer at room temperature for 15 min, rinsed in distilled H_2O, placed on SEM stubs using carbon tape, sputtered with a 5 nm layer of Pt, and imaged with a ZEISS Merlin FE-SEM with Gemini electron optics at 3 kV acceleration voltage and 100 pA probe current.

Introduction

Human cells reside in complex microenvironments with extracellular matrix components influencing cell fate through topographical, chemical, and mechanical cues. Accurately replicating bone tissue's nano- and microscale morphology and chemistry remains challenging, hindering biomimetic surface creation [1]. Thermal scanning probe lithography [2] (tSPL) shows promise for precise patterning, but practical limitations persist.

Results

Compatibility

We apply a thin film of thermosensitive poly methacrylate-carbamate-cinnamate copolymer (PMCC) resist to an ITO glass substrate and assess its ability to support the growth of human induced pluripotent stem cells (iMSCs) and withstand wet hydrolytic environment at 37 °C. PMCC effectively supports the culture of human iMSCs, similar to standard polystyrene tissue culture plastic (TCP). Both substrates enable rapid cell attachment, with cells displaying spindle-like morphology and comparable sizes one day after seeding, as shown by fluorescence staining of F-actin cytoskeletal filaments (Fig. 1). SEM images reveal filopodia extending from cells as connection points to the PMCC, crucial for cell adhesion and migration.

After 7 days of cell culture, calcein/ethidium homodimer 1 and acridine orange/propidium iodide stainings (Fig. 1i–n) show that the PMCC polymer supports cell culture as effectively as traditional TCP. Additionally, a PrestoBlue assay indicates higher metabolic activity for cells cultured on PMCC compared to TCP (Fig. 1p), ruling out any toxic effects of the PMCC resist on human iMSCs.

Increasing Throughput and Decreasing Cost

In the tSPL process, we use an AFM image of a demineralized bone tissue section [3] as a bitmap input and reproduce an array of these images to scale up the replica size. The high-quality replica confirms tSPL's capability to pattern complex quasi-3D tissue microenvironments with fidelity and resolution (Fig. 2). However, probe contamination during patterning significantly reduces the replica quality and resolution, ultimately hindering fur-

Figure 1

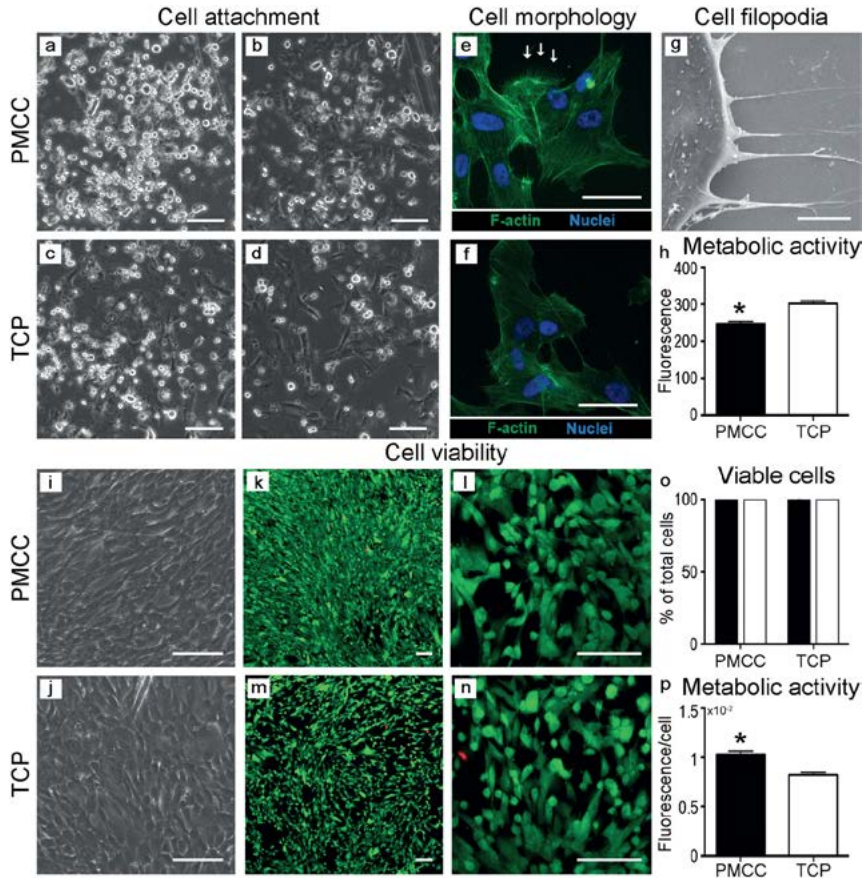

Fig. 1: *(a) Light micrographs of iMSCs attaching to PMCC resist and TCP at 2.5 and 5 h after seeding. b,c) Fluorescence and SEM images of iMSCs attached to PMCC resist and TCP 1 day after seeding, respectively. d) Metabolic activity of iMSCs on PMCC resist and TCP 1 day after seeding. e,f) Light images of iMSCs grown on PMCC resist and TCP one week after seeding. g) Confocal fluorescence images showing live (green) and dead (red) cells on PMCC resist and TCP after one week of culture. h) Percentage of viable cells on PMCC resist and TCP. i) Metabolic activity of iMSCs on PMCC resist and TCP after 1 week of culture. Scale bar: 50 µm (a)–(f), 5 µm (g), and 100 µm (i)–(n).*

Figure 2

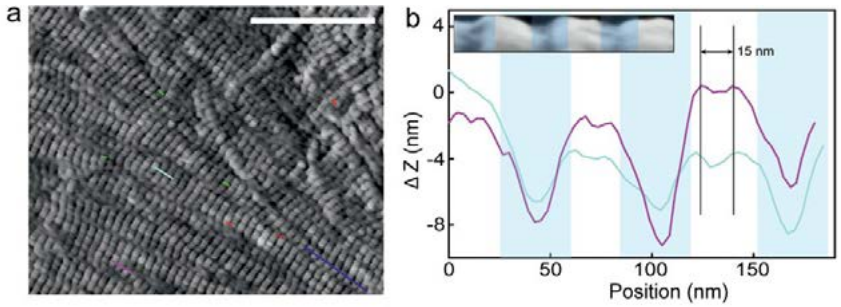

Fig. 2: *a) In situ tSPL thermal image of a bone tissue replica fabricated in PMCC resist. Scale bar: 1 µm. b) Cross-sectional profiles of two segments shown in (a).*

ther patterning. To address this, we adopt a threshold filtering strategy for the input image, reducing the need to change the thermal probe by 500%. The strategy involves setting a threshold to increase the number of 0-level pixels that do not require writing (and probe-surface contact). The replicated collagen fibrils display the characteristic twin-peak structure of fibril bumps, with a distance of ≈15–20 nm between them (Fig. 2b) [4].

Moreover, to reduce costs associated with numerous thermal probes for large-scale replicas, we introduce a probe washing procedure involving cleaning the probe in chloroform after every 7.7×104 µm of linear writing when using the filtered input image.

tSPL bone tissue replicas support human iMSC growth. A 0.2 mm x 0.05 mm replica on ITO glass with PMCC resist was tested for 3 days, showing cell migration, division, and multilayer formation. Nanopattern stability was confirmed after 3-day cell culture cycles, with no changes in grooves. PMCC adheres well to ITO glass over seven cycles, with <5% groove depth change and no compromise to pattern or cell compatibility.

Amine Functionality

tSPL replicates bone tissue topography and activates surface amine groups (Fig. 3a–c) [5]. Arrays of replicas are fabricated using different writing temperatures and pressures [6]. By labeling amine groups with Alexa 488, varying fluorescence intensities in each row of replicas indicate controlled local amine density (Fig. 3d–g).

Conclusion

Bio-tSPL is introduced as a solution to the challenges of tSPL throughput and cost. Smart software, post-patterning techniques, and a biocompatible polymer resist enable multiple cell culture cycles and tissue replica reusability, which was proved by techniques correlating electron and light microscopy from ZEISS. Bio-tSPL opens new avenues for understanding cell-tissue interactions, drug testing, and controlling stem cell fate for biomedical applications.

References

[1] Metavarayuth, K. et al. (2016). Influence of Surface Topographical Cues on the Differentiation of Mesenchymal Stem Cells in Vitro. *ACS Biomaterials Science and Engineering*. DOI: 10.1021/

Figure 3

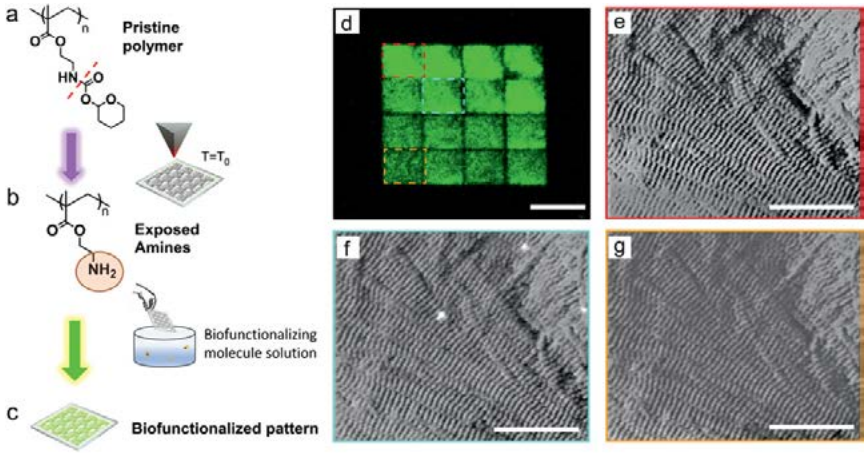

Fig. 3: *{a) Scheme of the tSPL patterning. b,c) Thermal exposure and biofunctionalization of the amine. d) Fluorescence microscopy image of an array of bone tissue replicas patterned using different probe temperatures and functionalized with Alexa 488 dye. Scale bar: 5 µm. e-g) In situ thermal topography images of individual tSPL replicas patterned with different probe temperatures. Scale bar: 1 µm. Each image corresponds to the color-coded dash-framed fluorescent pattern in (d).*

ACSBIOMATERIALS.5B00377/ASSET/IMAGES/LARGE/AB-2015-003773_0008.JPEG.

[2] Szoszkiewicz, R. et al. (2007). High-speed, sub-15 nm feature size thermochemical nanolithography. *Nano Letters*. DOI: 10.1021/NL070300F/SUPPL_FILE/NL070300FSI20070306_112213.PDF.

[3] Wallace, J.M. et al. (2010). Type i collagen exists as a distribution of nanoscale morphologies in teeth, bones, and tendons. *Langmuir*. DOI: 10.1021/LA100006A/SUPPL_FILE/LA100006A_SI_001.PDF.

[4] Greiner, J.F. et al. (2019). Natural and synthetic nanopores directing osteogenic differentiation of human stem cells. Nanomedicine: *Nanotechnology, Biology and Medicine*. DOI: 10.1016/J.NANO.2019.01.018.

[5] Bryant, S.J. et al. (2005). Incorporation of tissue-specific molecules alters chondrocyte metabolism and gene expression in photocrosslinked hydrogels. *Acta Biomaterialia*. DOI: 10.1016/J.ACTBIO.2004.11.003.

[6] Liu, X. et al. (2019). Sub-10 nm Resolution Patterning of Pockets for Enzyme Immobilization with Independent Density and Quasi-3D Topography Control. *ACS Applied Materials and Interfaces*. DOI: 10.1021/ACSAMI.9B11844/ASSET/IMAGES/LARGE/AM9B11844_0005.JPEG.

Additive manufacturing of porous biominerals

Adapted from Ran Zhao, Nina Kølln Wittig, Gaia De Angelis, *et al.* Article link

Nature forms hard functional materials from mineralized soft organic scaffolds. This study presents a room-temperature process combining localized mineralization with emulsion-based 3D printing to create cm-sized biominerals with pores ranging from hundreds of nm to mm in diameter. SEM images were recorded on a ZEISS GeminiSEM 300 operated at 3 kV with a working distance of approximately 8 mm. Samples were coated with 10 nm of gold to prevent charging effects.

EDX spectroscopy was acquired using the same ZEISS GeminiSEM 300 equipped with an Oxford Instruments EDX detector. It operated at 10 kV and 180 pA beam current, with an input count per second of around 3000 cps. The 3D morphology of printed samples was investigated using X-ray micro-computed tomography (µ-CT) with an Xradia 620 Versa X-ray microscope (ZEISS).

Introduction

Nature fabricates lightweight, porous biominerals with remarkable mechanical properties [1–3]. Achieving the controlled incorporation of pores across multiple length scales in synthetic mineral-based composites remains challenging [4,5]. Existing materials are either thin films [6,7] or dense bulk materials [8,9] not suitable for locomotive applications. Here, we introduce an emulsion-templated water-based biomineralization process for precise pore size control (hundreds of nm to mm scale).

Figure 1

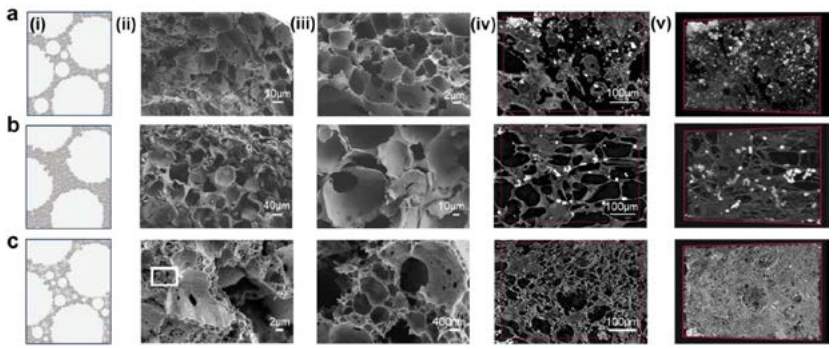

Fig. 1: *Microstructure of porous composites: (i) Schematic illustrations, (ii) SEM micrographs (overview), (iii) SEM micrographs (close-up), (iv) tomographic slices, and (v) 3D renderings of porous minerals made from a) vortexing-formed emulsions, b) microfluidic device-formed emulsions, and c) a mixture of two emulsion batches with different drop sizes. Samples contain 0.1 m Ca^{2+} and 5 wt% PVA in capsule-based inks. Red boxes in (iv) indicate central virtual slices of the 3D region of interest (ROI) in (v).*

Results

To control synthetic biominerals' pore size and distribution, we combine *in-situ* mineralization with emulsion-based 3D printing. Emulsion drops with diameters 200 nm - 120 µm were prepared by mixing a fluorinated oil with an aqueous solution containing $CaCl_2$ and poly(vinyl alcohol) (PVA). An amphiphilic block copolymer surfactant, end-functionalized with two pyrogallols, prevented emulsion coalescence [10,11].Tip sonication yielded polydisperse oil-in-water drops (100s nm diameter) with surfactants adsorbing and crosslinking with Ca^{2+} to form capsules.

Emulsion drops with broader size ranges (6 - 52 µm) were fabricated by vortexing the oil/water mixture, while microfluidic flow-focusing devices produced drops with narrower size distributions.

For larger-scale porous materials, we 3D-printed emulsion templates by up-concentrating drops through sedimentation, inducing shear-thinning behavior, crucial for 3D printing [12].

To create solid porous structures, selective mineralization was induced at capsule surfaces and in the surrounding aqueous solution. Capsules present pyrogallol functionalities, endowing high affinity for Ca^{2+} due to Ca^{2+} –pyrogallol interactions [13]. Minerals preferentially formed at the capsule surface [14–16], when capsules with high Ca^{2+} concentrations at their surfaces were immersed in

Figure 2

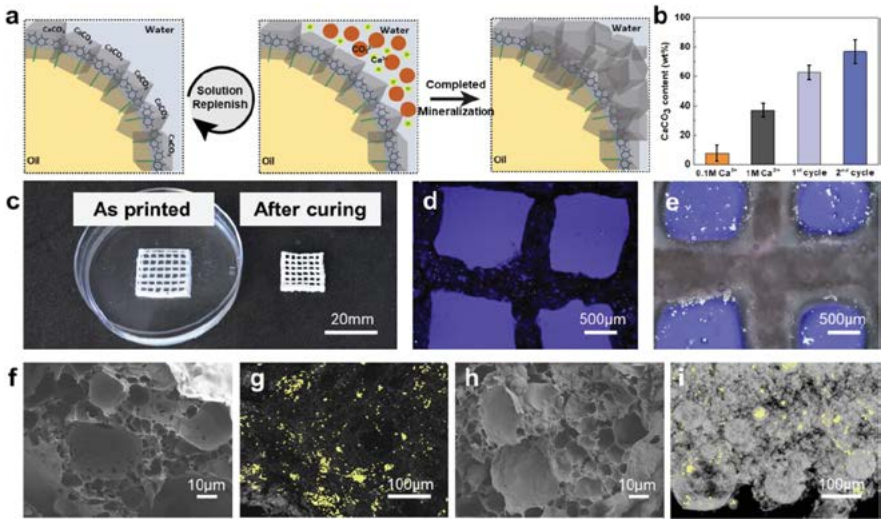

Fig. 2: *Curing of 3D printed structures: a) Schematic illustration of 3D printed $CaCO_3$ mineralization process through repeated replenishment of the aqueous bath with Ca^{2+} and a carbonate source. b) Influence of initial Ca^{2+} concentration and mineralization cycles on $CaCO_3$ weight fraction within the composite, determined through thermogravimetric analysis (TGA). c) Photograph of a 20 mm × 20 mm × 3 mm printed lattice after two mineralization cycles, showing low volume shrinkage and high shape fidelity. d,e) Polarized optical microscopy images of samples before (d) and after (e) three mineralization cycles. f,h) SEM images and g,i) 3D renderings of X-ray µ-CTs of samples without additional mineralization cycles (f,g), displaying interconnected pore structures, and after two additional mineralization cycles (h,i), revealing intact spherical mineral shells. Yellow parts in 3D renderings mark isolated pores.*

Figure 3

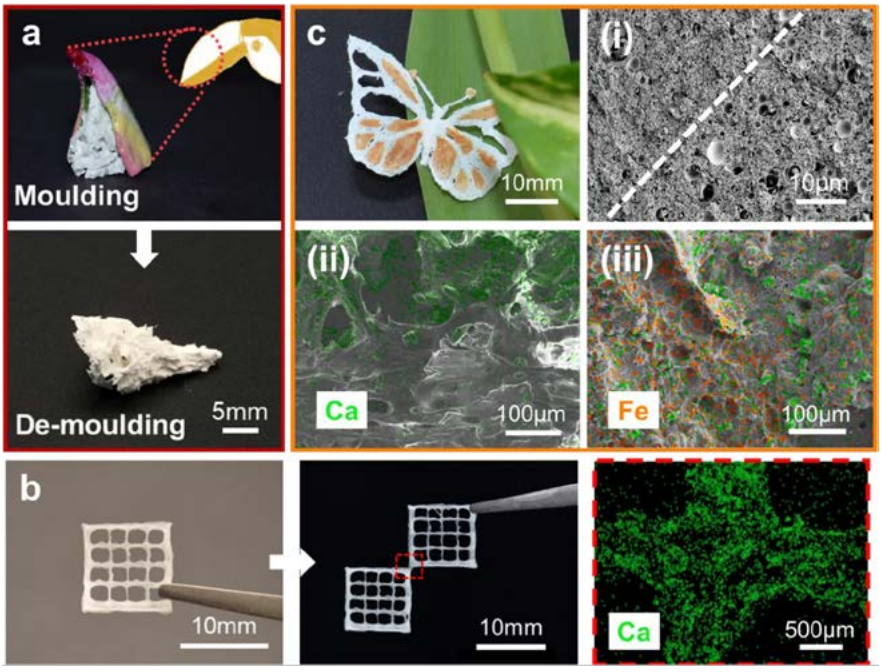

Fig. 3: *Proof of concept of 3D printed porous mineral-based composites: a) artificial toucan beak made by molding inks into a 3D printed shell, exhibiting well-defined morphology after demolding. b) Photograph of two printed mineralized lattices connected through an additional mineralization cycle, with corresponding EDX mapping of the connected part (red box). c) 3D printed butterfly produced by co-printing different capsule-based inks, sequentially mineralized. (i) SEM image of the cross-section showing local variations in pore sizes. The white dashed line indicates the boundary of the two co-printed inks. EDX mapping revealing (ii) the gradient in $CaCO_3$ concentration and (iii) presence of $Fe(OH)_3$.*

an aqueous solution containing a carbonate source. Mineral content increased rapidly within the first hour, plateauing thereafter. Storage modulus increase was primarily due to PVA gelation, and higher Ca^{2+} concentration increased mineralization.

Mineralized structures were air-dried, and observed through SEM. Pore diameters from vortexed emulsions ranged from 4 to 45 µm (Fig. 1a), slightly decreasing due to capillary forces causing shrinkage. Monodisperse emulsion drop templates showed a good correlation between drop and pore sizes, with pores averaging 87 µm and a 17 µm standard deviation (Fig. 1b). Emulsion stability prevented coalescence during 3D printing, resulting in mostly spherical pores (X-ray micro-computed tomography images in Fig. 1b iv,v). Figure 1c shows a porous sample from mixing two emulsions of different drop sizes, allowing control of pore size distribution by changing the volume ratio of the emulsions.

To address shrinkage, 3D-printed structures underwent repeated mineralization cycles (Fig. 2a). Shrinkage decreased linearly with more cycles (Fig. 2c), while $CaCO_3$ content increased with cycles (Fig. 2b). Samples with no cycles have interconnected open pores (Fig. 2f,g). Two cycles resulted in less interconnected spherical pores (Fig. 2h,i), but >2 cycles compromised shape fidelity as crystals grow out of printed filaments (Fig. 2d,e). We used two cycles for best shape fidelity and high mineral content.

An artificial toucan beak with a polymeric skin and porous mineral core was produced (Fig. 3a). The dried object is freestanding (Fig. 3b), indicating good connectivity. Calcium distribution at interfaces is homogeneous, shown by EDX mapping. In addition, a butterfly with wings composed of two inks with varying porosities was 3D printed (Fig. 3c). Co-printed inks with different capsules created a locally varying composition (Fig. 3c).

Conclusion

Capsule-based ink enables 3D printing of minerals with hierarchical porosity (100 nm to mm scale). Mechanical properties similar to natural minerals are achieved via adjustable mineralization conditions. The energy-efficient, aqueous process allows the incorporation of thermally labile substances. Additive supply controls mineral morphology and structure for desired mechanical properties.

References

[1] Aizenberg, J. et al. (2005). Materials science: Skeleton of euplectella sp.: Structural hierarchy from the nanoscale to the macroscale. *Science*. DOI: 10.1126/SCIENCE.1112255/ASSET/153826CD-4297-4E14-8785-E83A85285F71/ASSETS/GRAPHIC/309_275_F3.JPEG.

[2] Yang, T. et al. (2022). A damage-tolerant, dual-scale, single-crystalline microlattice in the knobby starfish, Protoreaster nodosus. *Science*. DOI: 10.1126/SCIENCE.ABJ9472/SUPPL_FILE/SCIENCE.ABJ9472_MOVIES_S1_TO_S5.ZIP.

[3] Chen, P.Y. et al. (2012). Biological materials: Functional adaptations and bioinspired designs. *Progress in Materials Science*. DOI: 10.1016/J.PMATSCI.2012.03.001.

[4] Song, J. et al. (2005). Mineralization of synthetic polymer scaffolds: A bottom-up approach for the development of artificial bone. *Journal of the American Chemical Society*. DOI: 10.1021/JA043776Z/SUPPL_FILE/JA043776ZSI20050106_121258.PDF.

[5] Ping, H. et al. (2022). Mineralization generates megapascal contractile stresses in collagen fibrils. *Science*. DOI: 10.1126/SCIENCE.ABM2664/SUPPL_FILE/SCIENCE.ABM2664_MOVIES_S1_AND_S2.ZIP.

[6] Xiao, C. et al. (2017). Total morphosynthesis of biomimetic prismatic-type $CaCO_3$ thin films. *Nature Communications*. DOI: 10.1038/s41467-017-01719-6.

[7] Chen, W. et al. (2020). Nacre-Inspired Mineralized Films with High Transparency and Mechanically Robust Underwater Superoleophobicity. *Advanced Materials*. DOI: 10.1002/ADMA.201907413.

[8] Mao, L.B. et al. (2016). Synthetic nacre by predesigned matrix-directed mineralization. *Science*. DOI: 10.1126/SCIENCE.AAF8991/SUPPL_FILE/PAPV2.PDF.

[9] Xin, A. et al. (2021). Growing Living Composites with Ordered Microstructures and Exceptional Mechanical Properties. *Advanced Materials*. DOI: 10.1002/ADMA.202006946.

[10] Etienne, G. et al. (2019). Bioinspired Viscoelastic Capsules: Delivery Vehicles and Beyond. *Advanced Materials*. DOI: 10.1002/ADMA.201808233.

[11] De Angelis, G. et al. (2023). From Surfactants to Viscoelastic Capsules. *Advanced Materials Interfaces*. DOI: 10.1002/ADMI.202202450.

[12] Daly, A.C. et al. (2019). Hydrogel microparticles for biomedical applications. *Nature Reviews Materials* 2019 5:1. DOI: 10.1038/s41578-019-0148-6.

[13] Charlet, A. et al. (2021). Shape retaining self-healing metal-coordinated hydrogels. *Nanoscale*. DOI: 10.1039/D0NR08351H.

[14] Hosoda, N. et al. (2003). Template effect of crystalline poly(vinyl alcohol) for selective formation of aragonite and vaterite $CaCO_3$ thin films. *Macromolecules*. DOI: 10.1021/MA025869B/ASSET/IMAGES/LARGE/MA-025869BF00006.JPEG.

[15] Li, Q. et al. (2016). Controlling hydrogel mechanics via bio-inspired polymer-nanoparticle bond dynamics. *ACS Nano*. DOI: 10.1021/ACSNANO.5B06692/ASSET/IMAGES/LARGE/NN-2015-066926_0006.JPEG.

16 Kim, S. et al. (2021). In situ mechanical reinforcement of polymer hydrogels via metal-coordinated crosslink mineralization. *Nature Communications*. DOI: 10.1038/s41467-021-20953-7.

BACK TO CONTENTS

Mechanically efficient cellular materials inspired by cuttlebone

Adapted from Anran Mao, Nifang Zhao, Yahui Liang, *et al.* Article link

Bioinspired 3D printing creates mechanically efficient cellular materials, crucial for aerospace, lightweight vehicles, and energy absorption. This study offers an effective approach for designing high-performance cellular materials. X-ray micro-CT (MicroXCT-200, ZEISS Xradia X-ray microscope, CA, USA) imaged 2 mm × 2 mm × 4 mm cuttlebone samples at a 2.5 µm voxel size.

Introduction

Biological materials like bamboo or cancellous bone have remarkable mechanical properties due to complex cellular structures [1,2]. Mimicking these features is sought after for next-generation efficient cellular materials [3–5]. The cuttlefish Sepia officinalis L. possesses a porous bone capable of resisting deep-sea hydrostatic pressure,[6] offering a mechanically efficient cellular structure. We 3D printed materials inspired by cuttlebone, sustaining a weight over 50,000 times their own.

Results

The cuttlefish uses its bone (Fig. 1a, b) as a rigid skeleton for movement and buoyancy control by pumping liquid in or out at different depths in seawater [7,8]. X-ray micro-computed tomography (CT) fully captured the cuttlebone's sophisticated architecture (Fig. 1d–f). Cuttlebone has a density of ~0.2 g cm^{-3} and 90% porosity. It comprises lamellae septa with continuously curved walls evenly distributed in each layer. The walls are 300–500 µm in height, 8–10 µm in thickness, and 80–180 µm in spacing (Fig. 1d).

Though lamellae septa and S-shaped walls have been reported [8,9], the mechanical function of asymmetrically wavy single walls was overlooked. Cross-sectional views of walls at the dorsal and ventral sides (parallel to the septa) show sinusoidal channels with similar periods (100–180 µm). However, their amplitudes differ significantly, with larger values at the ventral side (Fig. 1e, f).

Figure 1

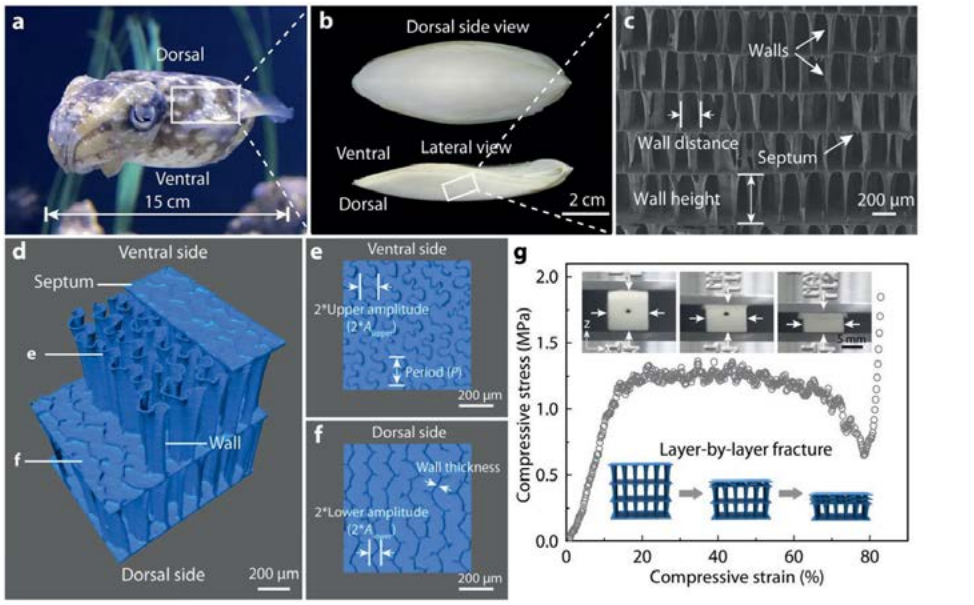

Fig. 1: *a,b) Optical images of a cuttlefish and cuttlebone. C) SEM image showing the multiscale architecture of cuttlebone. d) 3D structure of a two-layer model reconstructed from micro-CT images. e,f) Cross-sectional views of walls at the ventral (e) and dorsal (f) sides, with distinct amplitudes. g) Compressive stress–strain curve of cuttlebone.*

Figure 2

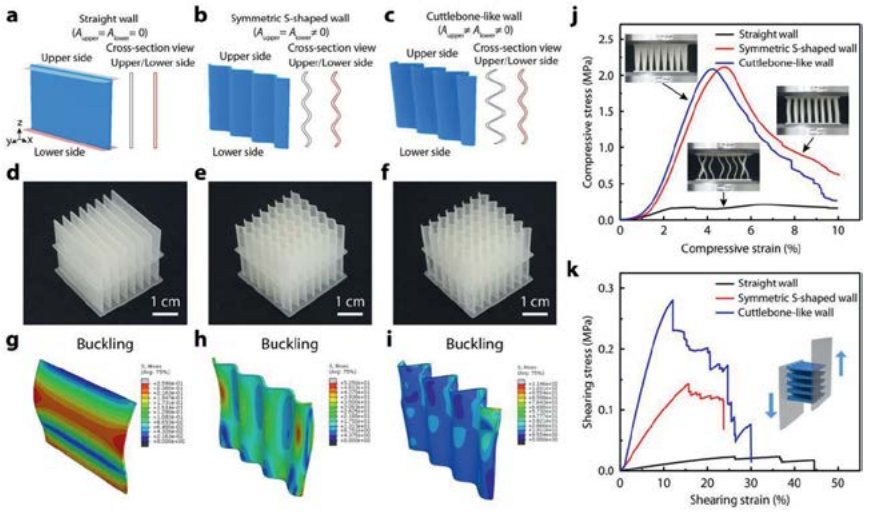

Fig. 2: *a–c) CAD designs of wall profiles. d–f) Optical images of 3D-printed models. g–i) FEM simulation of walls under compression. Models with straight (a,d,g), symmetric (b,e,h), and asymmetric (c,f,i) walls are compared. j) Compressive and k) shearing stress–strain curves for the three types of models.*

Cuttlebone (1 cm × 1 cm × 1 cm) was compressed perpendicular to its lamellar septa (Fig. 1g) under high hydrostatic pressure in deep seawater. Surprisingly, no obvious change in size occurred in the x-direction (ε_x) even with 50% compression in the z-direction (ε_z), showing a zero Poisson's ratio ($-\varepsilon_x/\varepsilon_z = 0$). The cuttlebone also exhibited directional densification, likely due to differencesin lamella height. Fracturing occurred successively from one layer to another. The compressive stress–strain curve (Fig. 1g) showed an elastic region of up to around 15% strain, followed by a long plateau of up to nearly 70% strain, with each fluctuation corresponding to individual layer fracture. A sharp rise due to densification occurred at a large strain (>80%).

Figure 3

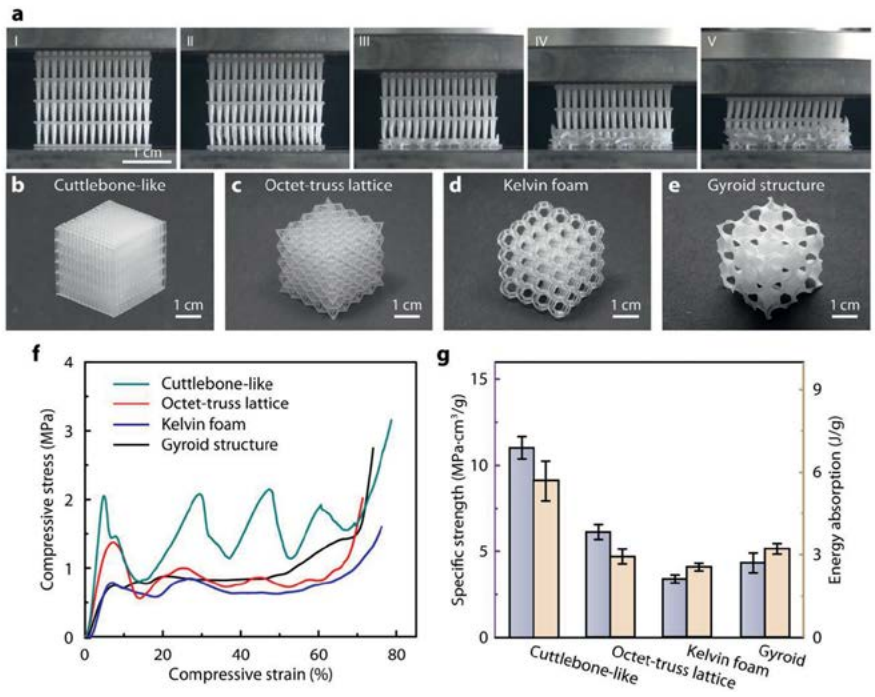

Fig. 3: *a) Optical images of 3D-printed multilayered cuttlebone-like material under uniaxial compressive test. b–e) Optical images of 3D-printed cellular materials with cuttlebone-like structure, octet-truss lattice, Kelvin foam, and gyroid structure. f) Stress–strain curves and g) statistics of specific strength and energy absorption of the four cellular materials in (b)–(e). Error bars represent standard deviations from at least five specimens.*

To study cuttlebone mechanics, we 3D-printed cellular materials mimicking cuttlebone architecture [10–12]. The models had lamellae layers with sinusoidal profiles, representing the simplified structural features of cuttlebone. Three models with different wall designs were compared (Fig. 2): a straight wall with zero amplitudes (Fig. 2a), a symmetric S-shaped wall with nonzero amplitudes on both sides (Fig. 2b), and a cuttlebone-like wall with different amplitudes on two sides (Fig. 2c). All models had the same distance between walls, height, thickness, and period, varying only in amplitude. FEM simulated the buckling process during compression.

The critical buckling stresses estimated by FEM (Fig. 2g–i) matched the experimentally measured ultimate compressive strengths (Fig. 2j). Changing straight walls to S-shaped walls increased compressive strength by tenfold, transitioning from global to local buckling. Models with S-shaped walls had no plateau in stress–strain curves due to having only one layer (Fig. 2j). The cuttlebone-like model, with high porosity, low density, and multiscale architecture, supported a weight over 50000 times its own. For shearing resistance, crucial during swimming, the cuttlebone-like model showed the highest strength, twice that of the symmetric S-shaped wall model, and ten times that of the straight wall model (Fig. 2k, 30 mm × 30 mm × 15 mm). These advantages in compression and shearing demonstrate the cuttlebone architecture's functional benefits for cuttlefish survival.

Inspired by these findings, we designed cuttlebone-like cellular materials which failed layer-by-layer under uniaxial compression (Fig. 3a), yielding a similar stress–strain curve as cuttlebone with a wide elastic region and a long plateau (Fig. 3f). The total fluctuations in the curve are consistent with the number of lamella layers. These observations clearly show that our bioinspired cellular material not only mimics the architecture of cuttlebone but also its mechanical behavior. The mechanical advantage of the cuttlebone-like structure is demonstrated by comparing with other typical porous structures including octet-truss lattice, Kelvin foam (tetrakaidecahedron lattice), and gyroid structure (Fig. 3b–e) [13–15]. With the same porosity and chemical

composition, the cuttlebone-like structure shows the highest specific strength and energy-absorption capability (Fig. 3f, g).

Conclusion

We studied the sophisticated architecture of cuttlebone and revealed its key role for simultaneously achieving high porosity and outstanding mechanical properties. Inspired by these findings, we developed a cuttlebone-like cellular material by 3D printing. With low weight, high strength, and excellent energy-absorption ability, this bioinspired cellular material may find wide applications in such as aerospace structures and implantable devices.

References

[1] Wegst, U.G.K. et al. (2014). Bioinspired structural materials. *Nature Materials*. DOI: 10.1038/nmat4089.

[2] Eder, M. et al. (2018). Biological composites—complex structures for functional diversity. *Science*. DOI: 10.1126/SCIENCE.AAT8297/ASSET/282146C3-DB5C-410C-AC80-4AF1B022376B/ASSETS/GRAPHIC/362_543_F4.JPEG.

[3] Flores-Bonano, S. et al. (2019). Tortuosity Index Based on Dynamic Mechanical Properties of Polyimide Foam for Aerospace *Applications. Materials*. DOI: 10.3390/ma12111851.

[4] Kausar, A. (2017). Polyurethane Composite Foams in High-Performance Applications: *A Polymer-Plastics Technology and Engineering Review*. DOI: 10.1080/03602559.2017.1329433.

[5] Hutmacher, D.W. (2000). Scaffolds in tissue engineering bone and cartilage. *Biomaterials*. DOI: 10.1016/S0142-9612(00)00121-6.

[6] Packard, A. (1969). Jet Propulsion and the Giant Fibre Response of Loligo. *Nature*. DOI: 10.1038/221875a0.

[7] Denton, E.J. and Gilpin-Brown, J.B. (1961). The Buoyancy of the Cuttlefish, Sepia Officinalis (L.). *Journal of the Marine Biological Association of the United Kingdom*. DOI: 10.1017/S0025315400023948.

[8] Birchall, J.D. and Thomas, N.L. (1983). On the architecture and function of cuttlefish bone. *Journal of Materials Science*. DOI: 10.1007/BF00555001/METRICS.

[9] Checa, A.G. et al. (2015). The cuttlefish *Sepia officinalis* (Sepiidae, Cephalopoda) constructs cuttlebone from a liquid-crystal precursor. *Scientific Reports*. DOI: 10.1038/SREP11513.

[10] Gu, G.X. et al. (2017). Hierarchically Enhanced Impact Resistance of Bioinspired Composites. *Advanced Materials*. DOI: 10.1002/ADMA.201700060.

[11] Raney, J.R. et al. (2018). Rotational 3D printing of damage-tolerant composites with programmable mechanics. *Proceedings of the National Academy of Sciences of the United States of America*. DOI: 10.1073/PNAS.1715157115/SUPPL_FILE/PNAS.1715157115.SM01.MP4.

[12] Porter, M.M. et al. (2015). Why the seahorse tail is square. *Science*. DOI: 10.1126/SCIENCE.AAA6683/SUPPL_FILE/PORTER-SM.PDF.

[13] Zheng, X. et al. (2014). Ultralight, ultrastiff mechanical metamaterials. *Science*. DOI: 10.1126/science.1252291.

[14] Yang, C. et al. (2019). 4D printing reconfigurable, deployable and mechanically tunable metamaterials. *Materials Horizons*. DOI: 10.1039/C9MH00302A.

[15] Pelanconi, M. and Ortona, A. (2019). Nature-Inspired, Ultra-Lightweight Structures with Gyroid Cores Produced by Additive Manufacturing and Reinforced by Unidirectional Carbon Fiber Ribs. *Materials*. DOI: 10.3390/MA12244134.

Evaluation of the engineered polysaccharide alpha-1,3 glucan in a thermoplastic polyurethane model system

Adapted from Jorge Wu Mok, Natnael Behabtu, Christian Lenges, *et al.* Article link

Enzymatic polymerization is under development as novel scalable process technology to convert sucrose to engineered polysaccharides. This study explores the impact of alpha-1,3 glucan as an additive in a thermoplastic polyurethane model system. Based on the observed property enhancements, engineered polysaccharides provide a sustainable performance additive for polyurethane materials.

For the X-ray tomography, a small strip of film (width 2 mm) was cut at room temperature and mounted in the sample holder. The samples were run on a ZEISS Xradia 510 Versa (50 kV, 4 W; 40×; voxel size: 0.40 um; 4–7 s exposure time; 2001 images collected). The images were reconstructed into 8-bit txm (ZEISS proprietary format) files and processed in ORS Dragonfly Pro with no filtering.

Introduction

Polyurethanes are essential in modern technologies [1–3], but achieving renewable building blocks with performance benefits, cost-effectiveness, and scalable production is challenging. Polysaccharides offer renewable materials with hydroxyl groups capable of reacting with isocyanate to form polyurethane bonds. Enzymatic polymerization enables the controlled synthesis of alpha-1,3-polyglucose (glucan) directly from sugars [4–6], yielding a linear, semicrystalline, water-insoluble polysaccharide with alpha-1,3 linkages. Glucan typically consists of 800 glucose repeat units with a polydispersity in the range of 1.7–2.0 [6].

During enzymatic polymerization, alpha-1,3 glycosidic linked polymer chains associate via hydrogen bonding, forming a water-insoluble, hierarchical structure with primary particles that further aggregate into spherical particles (1–5 µm) (Fig. 1).

Glucan forms stable dispersions in polyether or polyester polyols, commonly used in synthesizing polyurethane materials, including thermoplastic polyurethanes (TPUs) and foams. The study analyzes the impact of glucan additive on TPU composite matrix morphology, providing guidance for its application in other polyurethane materials like elastomers and foam systems (Fig. 2) [7].

Figure 1

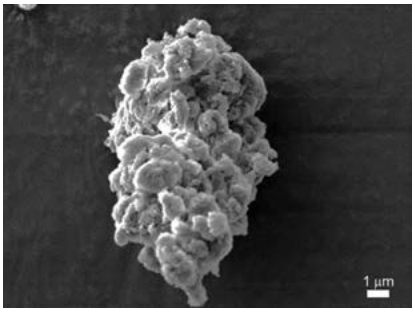

Fig. 1: *Scanning electron microscopy image of glucan polymer. Scale bar = 1 µm.*

Results

Glucan dispersions in polyols

Glucan was incorporated into TPU synthesis as stable dispersions in the polyol component. The unique spherical morphology of the polysaccharide

Figure 2

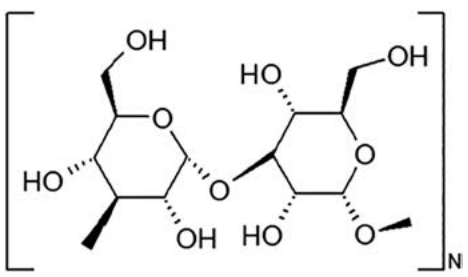

Fig. 2: *Structure of alpha-1,3-glucan.*

Figure 3

Fig. 3: *TPU reference (left) and TPU prepared with 6.2% glucan (right).*

structure from the water-based bioprocess was successfully maintained in the anhydrous polyol dispersion. The reactivity of the polysaccharide additive in the proposed TPU system was assessed by determining the hydroxyl value for a 10 wt% glucan dispersion in EO-capped PPG diol. The hydroxyl value of glucan in the polyol dispersion is 68.9 mg KOH/g, confirming its accessibility for reaction with isocyanate and incorporation into the polyurethane matrix.

TPUs synthesis and characterization

Glucan was incorporated into TPU synthesis as stable dispersions in the polyol component. The unique spherical morphology of the polysaccharide structure from the water-based bioprocess was successfully maintained in the anhydrous polyol dispersion. The reactivity of the polysaccharide additive in the proposed TPU system was assessed by determining the hydroxyl value for a 10 wt% glucan dispersion in EO-capped PPG diol. The hydroxyl value of glucan in the polyol dispersion is 68.9 mg KOH/g, confirming its accessibility for reaction with isocyanate and incorporation into the polyurethane matrix.

Analysis showed glucan's hydroxyl groups reacted with isocyanate. Solubilization study supported glucan's covalent bonding with TPU, potentially forming crosslinking points in the polyurethane matrix.

Thermal analyses of the reference TPU show it's amorphous with a negligible thermal transition at 185 °C, indicating no well-defined HS crystallinity. Transparency in Figure 3 aligns with this observation, as EO-capped PPG polyol is also amorphous. However, with 6.2 wt% glucan addition, a new crystalline HS domain forms, evident by the melt transition at 175 °C.
The polysaccharide particles contribute to the urethane HS network. TPUs with glucan are opaque due to the crystalline domain. Larger glucan particles with fewer hydroxyl groups resulted in transparent TPUs without the crystalline HS domain.

Figure 4 displays X-ray tomography images of the reference TPU and 6.2% glucan TPU, with image contrast based on material density difference. Glucan particles (lighter color) are well dispersed in the polyurethane (darker color). The control sample lacks contrast due to homogeneous density.

Glucan contributes to HS formation, thus should be considered in target HS calculation, increasing concentration from 38 to 44%. The polysaccharide-induced HS domain may affect physical and dynamic properties of resulting TPUs.

The reference TPU had a Shore A hardness of 59.4, while the 6.2% glucan TPU had 87.1; a meaningful increase suggesting the effect of the polysaccharide additive. Additionally, at 6.2% glucan, the overall tensile strength at 50%, 100%, 200%, and 300% elongation of the polyurethane matrix increased at 25 and 70 °C, attributed to glucan-induced crosslinking and HS crystalline domain formation.

DMA analyses showed glucan had no significant effect on the low temperature glassy state plateau. However, storage modulus data indicated a shift to higher temperatures for the transition to the rubbery state, with a higher rubbery state plateau modulus due to glucan-induced cross-linking and new HS formation.

Figure 4

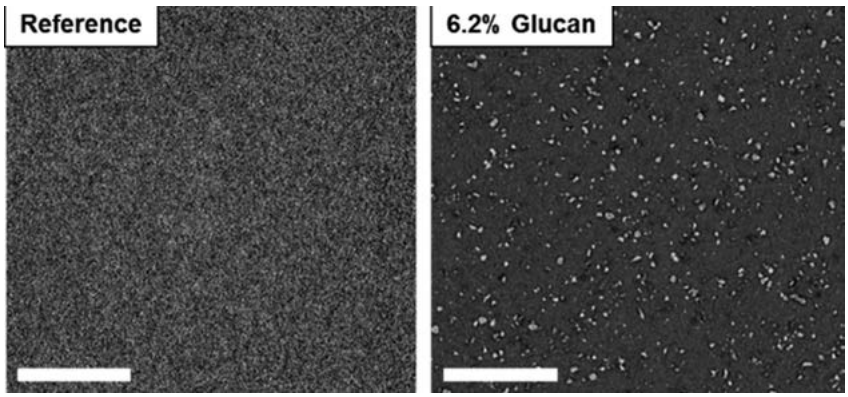

Fig. 4: *X-ray tomography images of reference and 6.2% glucan thermoplastic polyurethanes. Scale bar = 100 µm.*

Conclusion

In TPU synthesis, glucan reacts with isocyanate, leading to grafting and crosslinking in the polyurethane matrix. The covalent bonding of the polysaccharide to isocyanate forms a crystalline HS domain, influencing the resulting polyurethane's physical, thermal, and dynamic properties.

This study shows that glucan particles in polyether polyols act as reactive additives in TPUs, inducing a unique combination of covalent and crystalline HS crosslinking in the polyurethane matrix. This leads to improved performance and the potential to replace traditional TPU components with a sustainable additive. Furthermore, polyol dispersions of glucan can be used in other polyurethane products, including elastomers and foams, which is the focus of our ongoing research
.

References

[1] Herrington, R. et al. (1997). *Flexible polyurethane foams*, Dow Chemical Midland, Midland SE -.
[2] White, E.F.T. (1986). Polyurethane handbook Edited by G. Oertel, Hanser Publishers, Munich, 1985. pp. 629, price E104.70. ISBN 3-446-13671-1. *British Polymer Journal*. DOI: 10.1002/PI.4980180626.
[3] https://www.k-online.com/en/Media_News/News/K_Archive/2012_End-Use_Market_Survey_on_the_Polyurethanes_Industry.
[4] Kobayashi, S. et al. (2001). In vitro synthesis of cellulose and related polysaccharides. *Progress in Polymer Science*. DOI: 10.1016/S0079-6700(01)00026-0.
[5] https://patents.google.com/patent/US9926541B2/en.
[6] https://patents.google.com/patent/US7000000B1/en.
[7] https://patents.google.com/patent/WO2018017789A1/en.

Phototunable *Morpho* butterfly microstructures modified by liquid crystal polymers

Adapted from Xin Qing, Yuyun Liu, Jia Wei, *et al.* Article link

The unique hierarchical microstructures of the *Morpho* butterfly wing (MBW) exhibit angle independent blue iridescence. Here, a phototunable PhC is fabricated by depositing the azobenzene-containing linear liquid crystal polymer (LLCP) onto the MBW template. This phototunable PhC (Photonic crystals) may have potential applications in pigments, cosmetics, and sensors.

The morphology of microstructures before and after UV irradiation (10 mW cm^{-2}) was measured by a field emission scanning electron microscope (ZEISS FESEM, Ultra 55 and Sigma) at an accelerating voltage of 3 kV.

Introduction

Photonic crystals (PhCs) have periodic microstructures with a photonic bandgap that prohibits light propagation at specific wavelength [1], creating colorful reflective effects in nature [2]. Techniques like lithography and self-assembly have enabled PhC fabrication, but complex natural structures like *Morpho* butterflies' wings (MBW) pose challenges [2]. MBW's angle-independent blue iridescence has potential applications in various fields [3–5]. Instead of fully reconstructing the structures, modifying MBW with responsive coatings retains its delicate microstructures and optical properties [6,7] while allowing tunable reflection to external stimuli.

Crosslinked liquid crystal polymer (CLCP) is a promising responsive coating to induce substantial deformation of MBW microstructures. It combines mesogen units and polymer networks, giving it impressive mechanical properties and deformability [8,9]. Adding photochromic moieties (e.g., azobenzene) to CLCP allows it to respond to light, enabling localized, remote, and isothermal triggering and actuation [10].

Results

We report a new phototunable PhC by coating azobenzene-containing linear liquid crystal polymer (LLCP) onto MBW through electrospinning, achieving a photoresponsive LLCP-MBW composite. The fabrication process is illustrated in Figure 1a. A 5 wt% LLCP solution in dichloromethane was optimized for uniform electrospinning onto MBW without any pretreatment. The microscale LLCP fibers were melted at 120 °C into a thin coating, followed by annealing in the liquid crystal (LC) phase at 55 °C for half an hour, orienting the azobenzene mesogens in the LLCP layer [11].

Field emission scanning electron microscope (FESEM) was applied to investigate the topological change of the samples during the fabrication process. It was shown that the diameter of the obtained LLCP fibers through electrospinning was around 1 μm, which was close to the dimension of the MBW microstructure (Fig. 1b medium). The morphology of LLCP-coated *Morpho* butterfly wing (LLCP-MBW, Fig. 1b right) appeared similar to the original MBW (Fig. 1b left) without visible damage of the parallel-aligned ridges, proving that the microstructures were kept intact after modification. Compared to the IR absorbance of MBW, the new peak at 1730 cm^{-1} assigned to the —C=O stretching vibration of the carboxylic ester of LLCP was observed in LLCP-MBW (Fig. 1d), elaborating the presence of the melted LLCP fibers on the surface of the photonic structures. Next, the influence of LLCP on the reflectance of MBW was analyzed by reflectance spectrometer (Fig. 1e). The untreated MBW exhibited a strong reflection peak at 460 nm, while the LLCPMBW showed a broader and a bit lower reflection peak shifted to 470 nm, suggesting a thin layer of LLCP on the surface of MBW slightly changed the effective refractive index [12].

To study reflectance variation induced by photodeformation of hierarchical structures on LLCP-MBW, we used a super-resolution digital

Figure 1

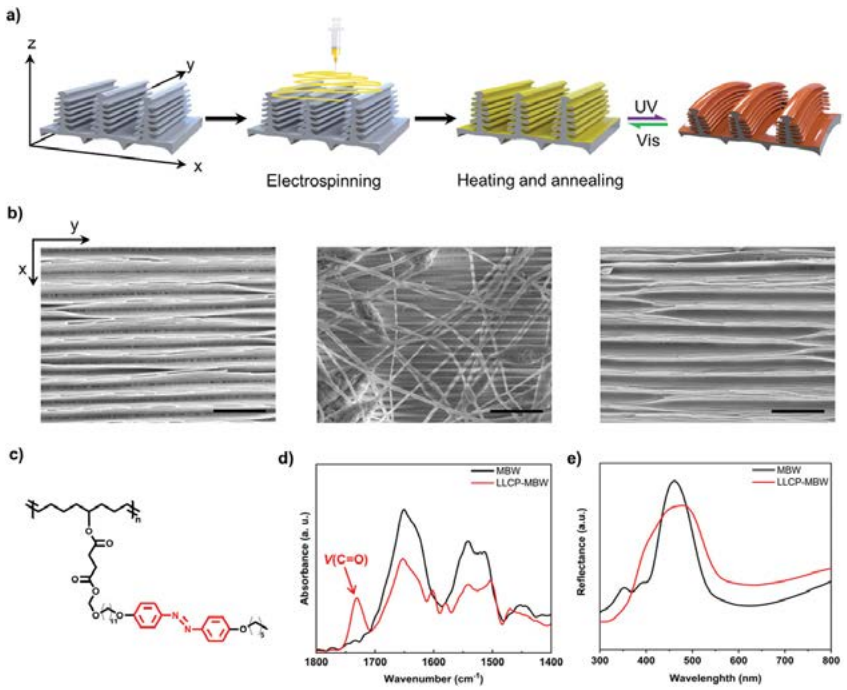

Fig. 1: *a) Schematic of LLCP-coated Morpho butterfly wing (LLCP-MBW) fabrication and reversible photoinduced deformation. b) SEM photos showing microstructures on MBW before electrospinning (left), after electrospinning (middle), and after heating and annealing (right). Scale bar, 5 μm. c) Chemical structure of photoresponsive LLCP with azobenzene mesogens. d) ATR-FTIR spectra of MBW (black) and LLCP-MBW (red) in the 1800–1400 cm^{-1} region. e) Reflective spectra of MBW (black) and LLCP-MBW (red).*

Figure 3

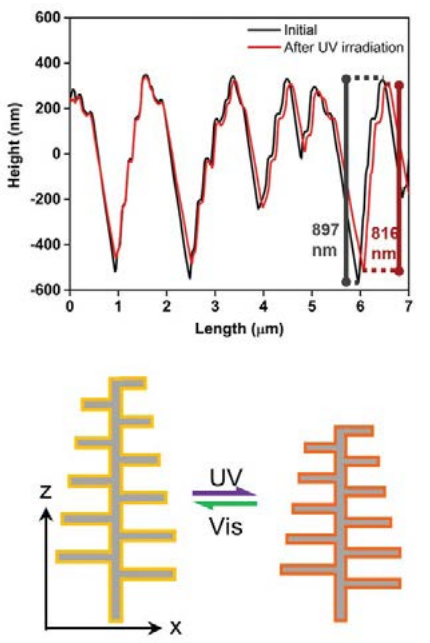

Fig. 3: *Surface profiles of the microstructures before (black line) and after (red line) UV irradiation (upper) and schematic illustration of the expansion perpendicular to the ridges and shrinkage vertical to the ridges (lower). UV light: 365 nm, 10 mW cm^{-2}. The irradiation time was 10 s for AFM and 20 s for FESEM, respectively.*

microscope. Blurred scales became clear upon UV irradiation and restored after UV off, indicating reversible height change. 3D reconstruction (Fig. 2) showed scales' tilted angle decreased up to 4 μm upon UV irradiation.

AFM revealed (–6.9 ± 1.3%) height reduction of ridges on LLCP-MBW scales after UV irradiation, with the maximum observed decrease around 80 nm (Fig. 3). UV irradiation caused trans–cis isomerization of azobenzene mesogens, shrinking LLCP layer thickness in z-axis and expanding in LLCP x–y plane. This led to in-plane expansion of LLCP, causing the nonphotoresponsive chitin MBW to bend away from the light source [13], resulting in scales fixed to the substrate exhibiting height reduction. The z-axis shrinkage of LLCP layer reduced the thickness of the entire LLCP-MBW scale, contracting ridges and decreasing lamella spacing.

According to the Bragg equation [12], the reduction of the lamella spacing and the decrease of LLCP layer thickness would induce a blueshift of the reflection peak. Owning to the high extinction coefficient of the trans-azobenzene at 365 nm [14], only the top few layers of the lamella structures in LLCP-MBW absorbed the incident light and deformed into smaller layer spacing, generating a new reflection peak at 397 nm. With the increase of light intensity, UV light penetrated deeper to deform the lower layers, enhancing the reflection intensity at 397 nm.

Figure 2

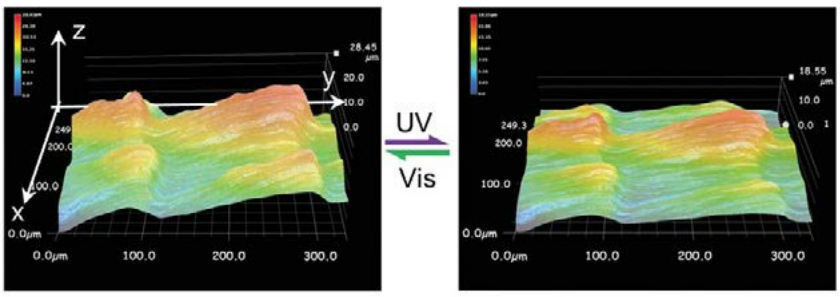

Fig. 2: *3D reconstruction images of the scales on the LLCP-MBW show the reversible deformation of the scales on LLCP-MBW upon UV (365 nm, 10 mW cm^{-2}) and visible light (white light from the microscope) irradiations.*

Conclusion

Electrospinning coating technology was used here to directly deposit a thin layer of LLCP with high molecular weight on MBW, preserving the delicate photonic structures of MBW. This work sets up a moderate and effective strategy to combine the natural biotemplates and responsive LLCP to fabricate complex responsive microstructures. Furthermore, through a better understanding of the structure–reflection relationship of the MBW-based PhCs, we anticipate that the phototunable PhC will be used in a variety of applications ranging from sensors, photo chromic pigments, anticounterfeiting to information storage technologies.

References

[1] Zhao, Y. et al. (2012). Bio-inspired variable structural color materials. *Chemical Society Reviews. Rev*. DOI: 10.1039/C2CS15267C.

[2] Dumanli, A.G. and Savin, T. (2016). Recent advances in the biomimicry of structural colours. *Chemical Society Reviews*. DOI: 10.1039/C6CS00129G.

[3] Han, Z. et al. (2016). Active Antifogging Property of Monolayer SiO^2 Film with Bioinspired Multiscale Hierarchical Pagoda Structures. *ACS Nano*. DOI: 10.1021/ACSNANO.6B03884/ASSET/IMAGES/LARGE/NN-2016-03884Q_0009.JPEG.

[4] Fang, J. et al. (2018). Three-Dimensional CdS/Au Butterfly Wing Scales with Hierarchical Rib Structures for Plasmon-Enhanced Photocatalytic Hydrogen Production. *ACS Applied Materials and Interfaces*. DOI: 10.1021/ACSAMI.8B03064/ASSET/IMAGES/LARGE/AM-2018-030644_0008.JPEG.

[5] Fei, X. et al. (2017). A bioinspired poly(N-isopropylacrylamide)/silver nanocomposite as a photonic crystal with both optical and thermal responses. *Nanoscale*. DOI: 10.1039/C7NR05087A.

[6] Shen, Q. et al. (2015). Subtractive Structural Modification of *Morpho* Butterfly Wings. *Small*. DOI: 10.1002/SMLL.201500502.

[7] Kinoshita, S. et al. (2002). Mechanisms of structural colour in the *Morpho* butterfly: cooperation of regularity and irregularity in an iridescent scale. *Proceedings of the Royal Society of London. Series B: Biological Sciences*. DOI: 10.1098/RSPB.2002.2019.

[8] Ohm, C. et al. (2010). Liquid Crystalline Elastomers as Actuators and Sensors. *Advanced Materials*. DOI: 10.1002/ADMA.200904059.

[9] Yu, Y. and Ikeda, T. (2006). Molecular Devices Soft Actuators Based on Liquid-Crystalline Elastomers. *Angewandte Chemie International Edition*. DOI: 10.1002/anie.200601760.

[10] Ube, T. and Ikeda, T. (2014). Photomobile Polymer Materials with Crosslinked Liquid-Crystalline Structures: Molecular Design, Fabrication, and Functions. *Angewandte Chemie International Edition*. DOI: 10.1002/ANIE.201400513.

[11] Lv, J.A. et al. (2016). Photocontrol of fluid slugs in liquid crystal polymer microactuators. *Nature*. DOI: 10.1038/nature19344.

[12] Fenzl, C. et al. (2014). Photonic Crystals for Chemical Sensing and Biosensing. *Angewandte Chemie International Edition*. DOI: 10.1002/anie.201307828.

[13] Kondo, M. et al. (2006). How Does the Initial Alignment of Mesogens Affect the Photoinduced Bending Behavior of Liquid-Crystalline Elastomers? *Angewandte Chemie International Edition*. DOI: 10.1002/anie.200503684.

[14] Yu, H. and Ikeda, T. (2011). Photocontrollable Liquid-Crystalline Actuators. *Advanced Materials*. DOI: 10.1002/adma.201100131.

BACK TO CONTENTS

A passion for utilizing nature-inspired materials to address global challenges

Interview with Associate Professor Erlantz Lizundia

In this interview, we delve into the world of Associate Professor Erlantz Lizundia, a prolific author who is revolutionizing the field of materials science. Erlantz's deep passion for science and technology is palpable as he discusses his journey from studying engineering to conducting groundbreaking research in renewable and biodegradable polymers. Through his innovative work, Erlantz endeavors to harness the power of natural materials to enhance our daily lives. As co-author of one of the articles featured within this collection, "Hierarchical Nanocellulose-Based Gel Polymer Electrolytes for Stable Na Electrodeposition in Sodium Ion Batteries", he discusses the critical importance of environmental considerations in materials development, the development fabrication of a cutting-edge bio-based gel electrolyte for zinc-ion batteries, and more! Prepare to be inspired.

What inspired you to pursue a degree in Advanced Materials Engineering?

I have been always fascinated by science and technology and how nature's mechanisms can yield materials and structures with such varied properties. In this manner, we can use the resources and materials that nature offers us, and through diverse chemical and physical modifications, obtain tailored functionalities that can improve the quality of our lives. The recent advances in materials science are being proven key to solving some of the most urgent global challenges that our society faces. Besides, considering that my region has a strong metallurgical tradition, it seemed like a logical way to go, with many job opportunities.

Where did you go to university and what factors influenced your decision to pursue your studies?

I did my university studies in Bilbao (Basque Country, north of Spain), very close to my hometown. Therefore, I was in a very familiar environment. The truth is that during my bachelor's degree, I was mostly involved in electronics, electrical engineering, and mechanical engineering and design. Therefore, I did not have much opportunity to interact with biological materials during this period. During my master's degree, I had several courses on polymers, opening a window to such versatile and mysterious materials. As I lived surrounded by great natural landscapes and forests, all this background helped me to think of new routes for the study and exploitation of renewable resources.

What career trajectory did you follow since graduating?

Once I completed my university studies, I worked in the private sector for two different periods. Right after finishing my bachelor's degree, I worked in a small-sized engineering consulting company on the design of metallic parts for the automotive industry. Afterward, I went back to the University for my master's and doctoral studies and once finished, I moved into a Research Center focused on machine tooling. This experience gave me a broader vision regarding the need for materials in practical applications. Later I went back into academia for a Postdoc at the Department of Physical Chemistry, with two additional visiting periods at Prof. Mark MacLachlan´s group (University of the British Columbia, Canada) and Prof. Markus Niederberger´s group (ETH Zürich, Switzerland). In 2016, I secured a position as Assistant Professor, and I was promoted to Associate Professor in 2021.

Can you provide an overview of your research on the use of renewable biological resources for the development of multifunctional nanohybrids?

I really believe that biological materials are nearly perfect and that much of their potential has yet to be exploited. In my research, we focus on the use of materials of renewable origin, mainly polymers. We seek ways to extract/isolate these polymers by relatively simple, scalable, and environmentally sustainable methods. We then process them by various methods to get different

Interview conducted by Róisín Murtagh, Editor at Wiley Analytical Science.

shapes and morphologies and study their structure/property relationships. Finally, we exploit their exceptional characteristics in areas that represent the major global challenges that face our society, including energy storage or environmental remediation. As for certain cases the properties of biopolymers need to be improved, we incorporate nanoparticles of distinct characteristics to provide nanohybrids with additional functionalities.

How do you approach designing experiments in your research, and what are some of the key considerations?

Whenever possible we look to nature for inspiration, and we investigate the way nature looks for solutions. For example, some crustaceans display iridescent colors without the need for pigments or dyes thanks to a specific hierarchical structure. So, can we apply this feature to develop more sustainable photonic sensors? Another of our mottos is that we can use renewable and biodegradable materials for a multitude of applications while keeping competitive processability, thermo-mechanical and electrochemical performances. Besides, bio-based polymers have a plethora of functional groups that can be easily tailored for controlled interaction with their surroundings. The exploitation of the hydrophilic character of polysaccharides, for example, leads to hydrogels that can efficiently dissociate salts, opening new routes for electrolytes in zinc-ion batteries. We are now also looking for minimal processing of biological resources, where it is possible to obtain materials with acceptable thermal, mechanical, and electrochemical properties after simple yet economically/environmentally sustainable processes.

How do you apply an eco-design approach in your work on developing novel materials and technologies, such as energy storage and polymer upcycling?

We aim at considering the environmental aspects during all the life-cycle stages so the environmental impacts can be minimized. During this process, we look at the origin and the extraction required for raw materials, their processing/synthesis, use-phase, and importantly, end-of-life. So, we do not only try to minimize environmental impacts during material production following the Green Chemistry principles, but we also seek to use locally available renewable materials, and we design towards enhanced operation lifespan of products. As most of the materials we are using are bio-based, we also ensure that upon disposal, these devices will biodegrade and will not leave harmful by-products. We also complete our studies with actual environmental footprint calculations using the life cycle assessment (LCA) methodology. This can help us, for example, to define the environmentally preferred route for recycling.

What is a recent breakthrough in your research about which you are particularly excited?

We are pleased to have achieved a battery that presents a particularly competitive electrochemical performance (mostly in terms of capacity and operation lifespan), while still exhibiting excellent degradability. Using a bio-based gel electrolyte, together with an organic cathode inspired by mussels, and packaging made by a marine polysaccharide, we obtained a zinc-ion battery that can disintegrate after completing its service life. In fact, the battery can disintegrate under composting conditions in by-products such as simple water-soluble sugars. Interestingly, we also avoid the need for critical raw materials or toxic electrolytes. This finding can help to circumvent the current contamination of marine and land environments induced by conventional batteries ending in marine or river environments.

What are some of the biggest challenges you face in your current research, and how are you working to overcome them?

Regarding "Hierarchical Nanocellulose-Based Gel Polymer Electrolytes for Stable Na Electrodeposition in Sodium Ion Batteries", the main objective of our work was to develop bio-based gel polymer electrolytes that offered stable Na electrodeposition. Batteries have a central role in the decarbonization of our society as they are essential to meet greenhouse gas emission targets. However, if we keep fabricating batteries using petroleum-derived polymers, or critical raw materials, the transition towards a sustainable circular economy may be jeopardized by a quick depletion of natural resources and environmental pollution caused by non-degradable materials. Besides, we think that further attention needs to be paid to enlarging the operation lifespan of batteries. This strategy of making batteries that can last for longer periods could be identified with a reuse strategy, which is the tightest loop of the circular economy and contributes to eliminating waste/pollution and reducing primary material consumption.

Therefore, we focused our attention on earth-abundant, bio-based, and biodegradable materials that besides offering competitive advantages over traditional fossil-derived materials have the potential to be biodegraded into innocuous by-products once their function is accomplished. It is amazing how nature offers us plenty of biological materials that are ready to be implemented in many of our daily applications. In the last years, we have explored many bio-derived polymers for battery applications, each of them with its own peculiarities of processing and properties. Obtaining a good balance between function and ease of processing of bio-based polymers results in a challenge because these materials must be well understood to exploit their full potential. For example, nanocelluloses offer intriguing self-assembly characteristics that can be used to obtain highly porous hydro- and aerogels using water as a dispersing media. Other bio-based polymers such as agarose or carboxymethyl cellulose, on the contrary, are better processed into films or used as binders. Therefore, understanding the specific characteristics of bio-based polymers is a very relevant step. In that particular work, we mixed stiff and short cellulose nanocrystals with flexible and long cellulose nanofibrils to obtain highly porous gel polymer electrolytes that offered a good resistance against dendrite growth while keeping a stable interface with metallic Na. We also tailored the porous structure to obtain mesopores that enabled uniform ion transference across the electrolyte, and we exploited the different functional groups of bio-based polymers to facilitate ion pair dissociation and increase the Na ion transference number. All this entails preparing numerous samples and gradually optimizing the targeted properties, one at a time.

How do sodium ion batteries based on earth-abundant materials contribute to a decarbonized society?

Sodium-ion batteries are composed of materials that are found abundantly and homogeneously around the globe. Actually, sodium is >1000 times more abundant than lithium, it is evenly distributed worldwide, and it is markedly cheaper than lithium. This reduces the dependence on foreign-world

countries for material acquisition, minimizes the need for long transportation, and can potentially yield cheaper batteries. Besides, sodium-ion batteries are more stable in the fully discharged state when compared with lithium-ion batteries, significantly improving the safety of stored batteries (of particular interest for large-sized batteries such as stationary applications). Importantly, the similarity of sodium and lithium enables the exploitation of the already existing (and up-scaled) industrial processes for sodium-ion battery fabrication. Not only this, but sodium-ion batteries can render a reduced life cycle CO_2 footprint per kWh of stored energy over benchmark lithium-ion batteries (according to life cycle assessment). However, there are still many challenges that need to be faced for the practical implementation of sodium-ion batteries, including a limited energy density, lower efficiency, and shorter lifespans.

What are the limitations of sodium-ion batteries compared to lithium-ion batteries in terms of energy density and operational lifetime?

Unfortunately, sodium has a theoretical capacity that remains well below the one shown by lithium. Also considering that sodium-ion batteries operate at a lower voltage than lithium-ion batteries, the specific energy densities in sodium-ion batteries often remain at 90-120 $Wh{\cdot}kg^{-1}$. This range is below the specific energy densities achieved for lithium-ion batteries, limiting the implementation of sodium-ion batteries in many applications, especially when volume and weight are limiting factors (i.e., electric vehicles). As such, big efforts are being focused to increase the energy density of sodium-ion batteries close to 250 $Wh{\cdot}kg^{-1}$, for example, by developing new cathode materials.

Another aspect to improve is the extension of the operational lifespan. Several interesting properties can be exploited in gel electrolytes to extend the operational lifetime of batteries. Firstly, replacing the conventional separator-liquid electrolyte pair with a gel-like electrolyte can avoid undesired liquid electrolyte leakage that prevents the battery from operating longer times. Secondly, gel polymer electrolytes offer a good compromise between room-temperature ionic conductivity and mechanical properties, protecting the battery from undesired dendritic puncture (short-circuit) while ensuring optimum electrochemical performance. Finally, the structural and physico-chemical interactions of gel polymer electrolytes can be controlled to make them mechanically conformable, which in turn enhances the compatibility with electrodes to extend operating lifetimes.

What are the most important considerations when selecting a microscope for gel polymer electrolyte (GPE) analyses?

Ideally, a microscope for GEP analyses should have a wide magnification range so it is possible to observe the morphology of the electrolytes at different length scales. This characteristic is particularly critical when working with hierarchical materials having nanoscale and microscale features. Obtaining high-magnification images with bio-based polymers is often complex as the electron beam can degrade the sample that is being observed. So, a microscope that can operate at low beam current and acceleration voltage is required.

What specific ZEISS instrument was employed to analyze the samples in this study, and how did it contribute to the findings?

In our research, we used a ZEISS SEM instrument, DSM 982 Gemini. It provided high-resolution imaging, which proved essential for observing all the details in our hierarchical gel electrolytes. As a matter of fact, it was possible to achieve low-magnification images to observe the microporous morphologies but also enable higher magnifications for analyzing individual filamentous cellulosic nanocrystals and nanofibers, which present diameters of 5 to 30 nm and lengths extending up to a few hundred nanometers. In addition, during our work with polymer electrolytes, we used the Energy Dispersive Spectroscopy (EDX) detector for post-mortem analyses. This helped us to observe the morphology and composition of the cycled electrolytes and metallic Na and understand the electrodeposition behavior.

Profile

Erlantz completed his Ph.D. in Advanced Materials Engineering at the University of the Basque Country in 2011. He currently works at the Life Cycle Thinking Research Group on renewable materials (cellulose, lignin, and chitin) for energy storage, environmental remediation, and packaging. Erlantz also uses life cycle assessment to assist in the design of environmentally sustainable materials and devices.

Affiliation: Life Cycle Thinking Group, Department of Graphic Design and Engineering Projects, Faculty of Engineering in Bilbao, University of the Basque Country (UPV/EHU), Bilbao, 48013 Spain.
ORCID: 0000-0003-4013-2721
Website: https://scholar.google.es/citations?hl=es&user=fDlHA4YAAAAJ
Social media: https://www.linkedin.com/in/erlantz-lizundia-3086b070/

Application Note

Characterization of the 3D Microstructure of Nanofibrous Scaffolds for Tissue Engineering

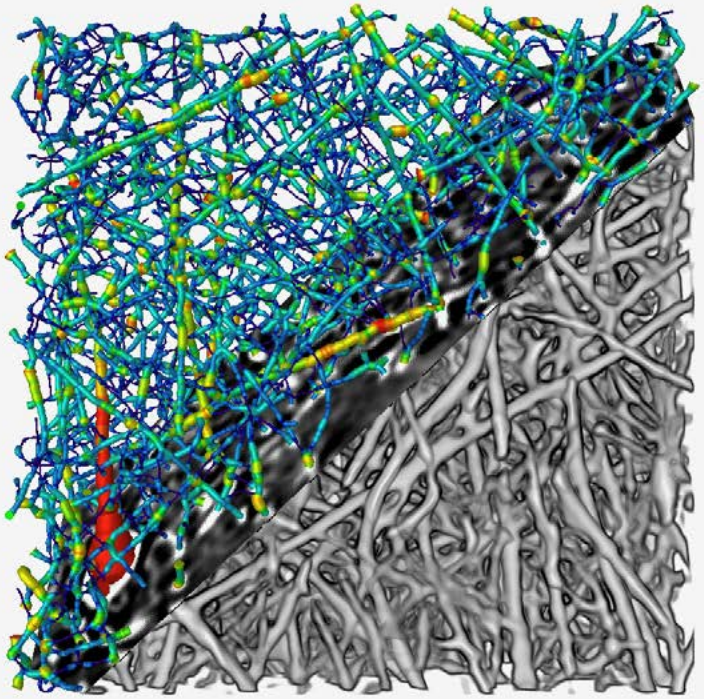

ZEISS

Seeing beyond

Authors: Juliana Martins de Souza e Silva, Cristine Santos de Oliveira, Ralf B. Wehrspohn
Microstructure-based Materials Design – mikroMD, Martin Luther University Halle-Wittenberg, Germany
Tobias Hedtke, Christian E. H. Schmelzer
Fraunhofer Institute for Microstructure of Materials and Systems IMWS, Halle (Saale), Germany
Fang Zhou
Carl Zeiss Microscopy GmbH, Oberkochen, Germany
Date: September 2020

Introduction

The discipline of tissue engineering aims to repair and regenerate damaged organs or tissues using tissue constructs created ex vivo. The major challenge lies in the design and fabrication of scaffolds that enable three-dimensional (3D) tissue growth or wound healing for clinical applications, e.g. facilitating the preparation of bioartificial transplants. Such scaffolds should be biocompatible for cells to adhere and possess high porosity and adequate pore size, which are both necessary to enable diffusion of nutrients and oxygen to cells throughout the whole structure. Biodegradability is often an essential requirement since some types of scaffolds should preferably be absorbed by the surrounding tissues at a proper rate without the necessity of surgical removal. Moreover, scaffolds should provide the desired form and architecture as well as certain mechanical stability to mimic and/or support the native tissue.

The visualization of the morphology and the characterization of the microstructures of the designed scaffold in 3D, like the porosity, pore size and fiber morphology, are crucial for the design and fabrication of tailored and application-optimized materials. The present application note is based on the research published in [1] and presents the X-ray microscopy (XRM) characterization of the cross-linked electrospun gelatin nanofibers that can be used e.g. as nanofibrous scaffold for skin regeneration, and skin wound dressing in medical care. The unique phase-contrast using Zernike phase plate for low atomic number materials in the laboratory-based X-ray microscope ZEISS Xradia 810 Ultra is discussed in detail.

Cross-linked Gelatin Nanofibrous Scaffold

Gelatin is a biodegradable and biocompatible natural biomaterial that can provide a good environment for cell attachment and spreading. Therefore, it is an eligible base material for tissue engineering.

Gelatin nanofibrous scaffolds were fabricated via the electrospinning technique as reported in [1]. The nanofibers show a random, nonwoven architecture with interconnected pores, which mimic the extracellular matrix of the native tissues like skin. To further stabilize the gelatin mat, it was exposed to a formaldehyde-rich atmosphere for different periods, which results in chemical cross-linking of the fibers and morphological changes of the mats due to fiber thickening.

3D Characterization of Cross-linked Gelatin Nanofibrous Scaffold using Phase-Contrast

3D characterization of the porous structure of the cross-linked gelatin scaffolds using X-ray microscopy is a challenge, because the gelatin nanofibers are composed of elements with low atomic number that deliver very low X-ray absorption-contrast. However, the visualization of the morphology and the characterization of sample features related to the 3D structure of gelatin scaffold, like the porosity and fibers thickness in the volume, is indispensable for the design and fabrication of tailored and application-optimized materials.

Xradia 810 Ultra equipped with a chromium source (5.4 keV) and integrated phase-contrast technology can be applied to enhance the 3D visibility of nanostructures of biopolymers with low absorption contrast.

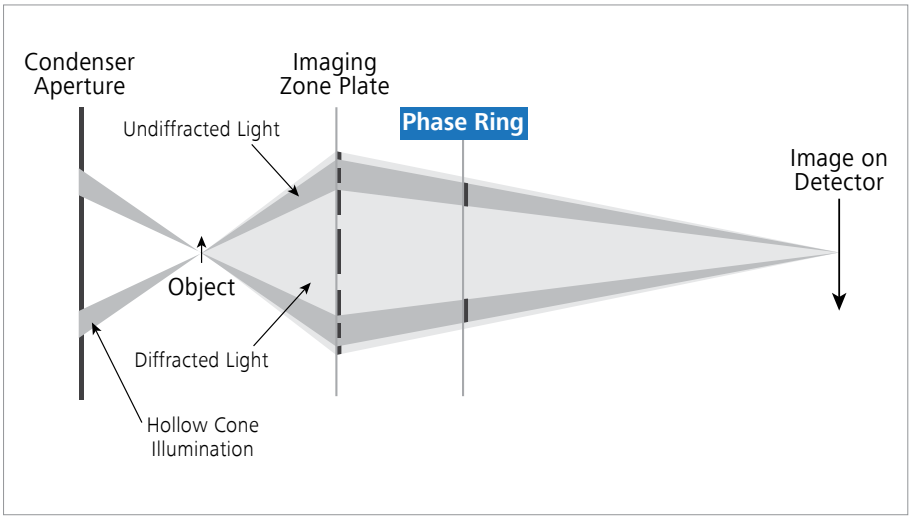

Figure 1 *The X-ray beam path of ZEISS Xradia Ultra 810. A phase ring is inserted between the Fresnel zone plate objective and the detector for unique Zernike phase-contrast in a laboratory setup.*

In this study, Zernike phase-contrast imaging using Xradia 810 Ultra was employed to visualize and characterize microstructures of electrospun nanofibrous scaffolds. In Xradia 810 Ultra the sample is illuminated by an annular beam and a phase ring is inserted in the beam path after the objective (cf. Fig. 1). The phase ring shifts the phase of the background light relative to the light scattered by the specimen. The interference of the two beams in the detector plane converts phase shifts into intensity variations detected downstream.

All samples were scanned with a total of 901 projection images (field-of-view of 64 µm²) acquired by rotating the sample over 180°. The exposure time was 30 s and a detector binning of 1×1 was used (isotropic voxel size of 64 nm³) for the thinner samples, which are the pristine and the samples cross-linked for 60 and 90 min. To reduce the scan time while keeping X-ray counts comparable, an exposure time of 15 s was used for imaging the thicker samples (cross-linked for 120 and 180 min), with a detector binning of 2×2. To correct any sample drift, the AMC (adaptive motion compensation) option included in the software of Xradia 810 Ultra was used. The AMC runs after the main scan a quick scan with a small number of projections that are later used to correct large sample drifts. The volumetric reconstruction of the dataset was done using XRM Reconstructor software integrated into Xradia 810 Ultra.

Fig. 2 shows the spatial distribution of the fibers in volumetric XRM images and their morphological changes with increasing cross-link duration. The presence and distribution of beads in the samples and the interaction with the surrounding fibers in the space can be easily visualized using the 3D dataset.

The diameter distribution for the fibers estimated using the 3D dataset is shown in Fig. 3. By means of the 3D XRM datasets, a trend of fiber diameter increase with increasing cross-linking time is observed. The thin pristine gelatin fibers merge with the cross-linking. The longer the cross-linking time, the more pronounced is the merging of the fibers and, at 120 min-long cross-linking, the mat does not resemble a fibrous structure anymore. The change of the fibers causes a change in the size and shape of the mat pores, which can be seen in Fig. 4, where individual pores are illustrated in different colors in 3D XRM datasets. A decrease in the size of the pores is observed progressively with increasing cross-linking duration, with a more pronounced total porous volume decrease at 120 min of cross-linking.

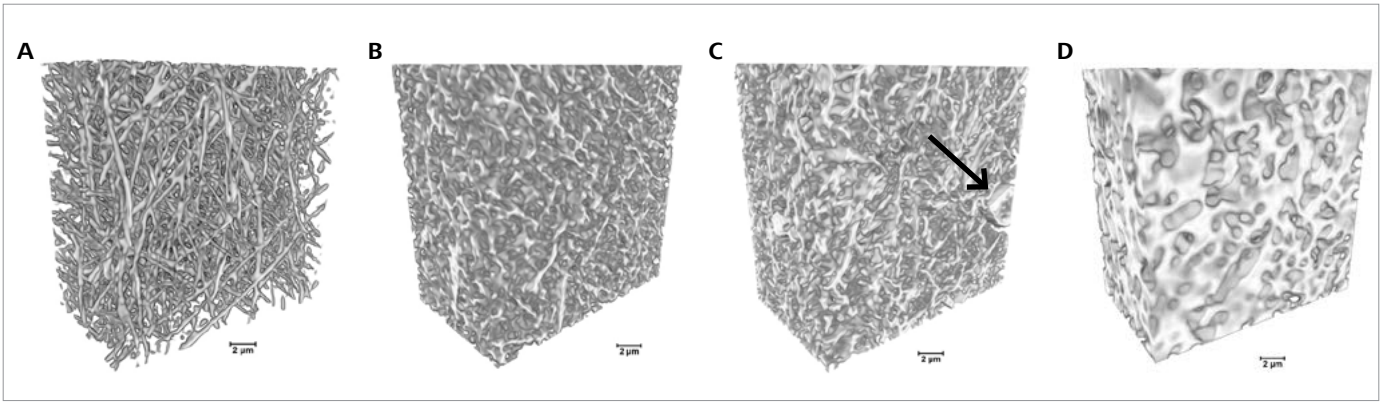

Figure 2 *3D imaging of electrospun gelatin fibers cross-linked for different times using Xradia 810 Ultra. The cross-linking duration increase from 0 min (pristine gelatin sample) to 60, 90, and 120 min from A to D , respectively. Arrow indicates a bead in the fibrous mats (scale bar: 2 µm).*

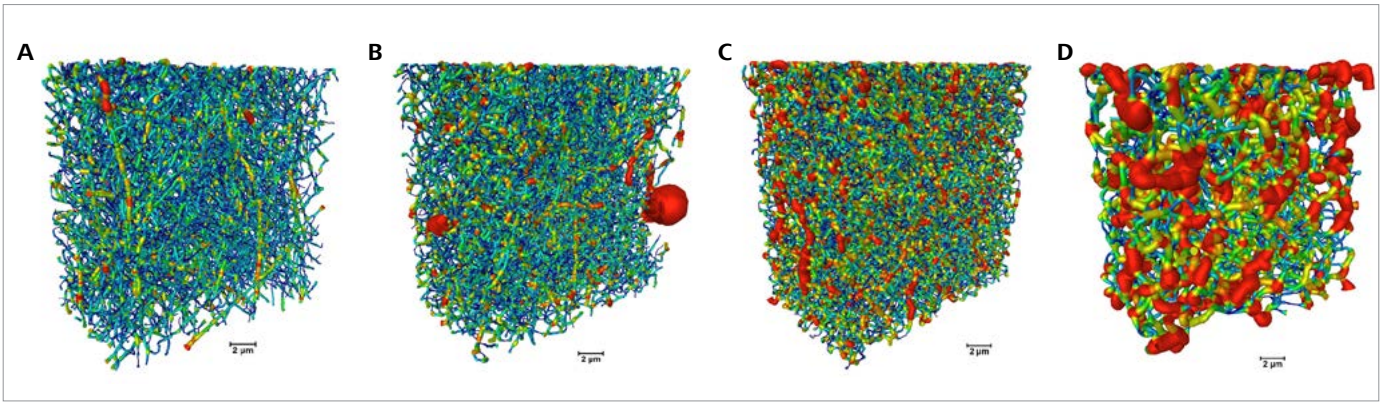

Figure 3 *Fiber characterization for samples cross-linked for different times (0 to 120 min from A to D, respectively). The volumetric color-maps encode the thickness of the fibers, which is correlated to the duration of cross-link (scale bar: 2 µm).*

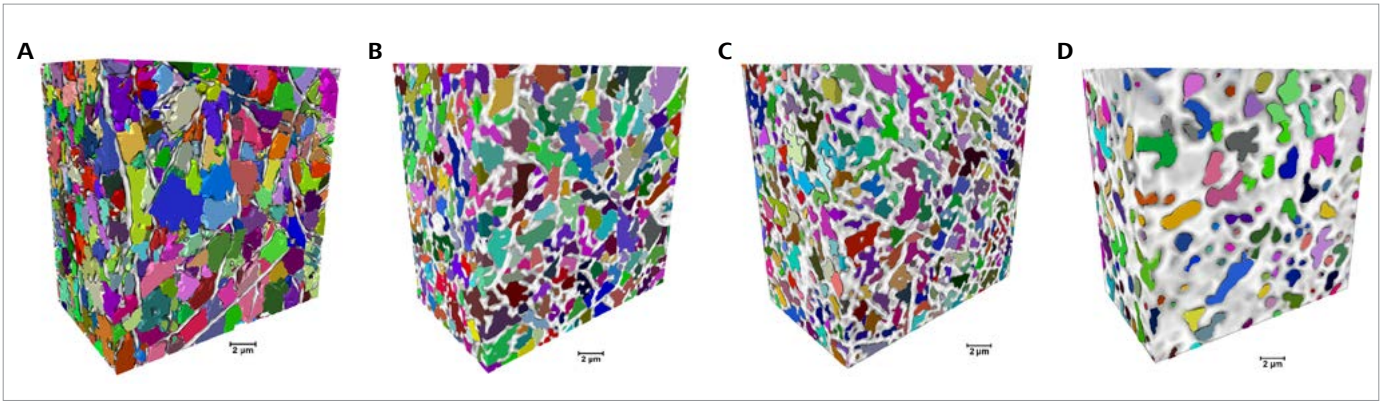

Figure 4 *Pore characterization for samples cross-linked for different durations (0, 60, 90 and 120 min from A to D, respectively). Volumetric representations of the fibers (white/gray) and the samples' pore distribution, with the separated pores represented in different colors (scale bar: 2 µm).*

Conclusion

Regeneration of damaged tissue via nanofibrous scaffolds requires designing an extracellular matrix-like scaffold with high surface area to volume ratio as well as high porosity for promoting homogeneous cell attachment and proliferation throughout the scaffold. Xradia 810 Ultra was successfully applied to characterize the morphology of electrospun gelatin fibers for understanding the effect of fiber cross-linking in the gelatin mat morphology.

Xradia Ultra 810 is a laboratory-based 3D X-ray microscope that enables non-destructive tomography with resolution better than 100 nm for biopolymer samples without the need of any special sample preparation protocol. Furthermore, Xradia 810 Ultra delivers phase-contrast imaging using a Zernike-type phase plate, which is unique for a laboratory microscope and enhances the quality of high-resolution imaging of low Z materials, such as biopolymers.

Phase-contrast imaging can be used to successfully characterize the morphology of biopolymer nanofibrous scaffolds and provides beneficial insights for the design and fabrication of novel fibrous materials.

Cover Image:

Image courtesy of Dr. C. Santos de Oliveira and sample courtesy of Fraunhofer Institute for Microstructure of Materials and Systems IMWS, Halle (Saale), Germany.

References

[1] C.S. de Oliveira, A.T. González, T. Hedtke, T. Kürbitz, A. Heilmann, C.E.H. Schmelzer, J. Martins de S. e Silva, Materials Science and Engineering: C, Volume 115, October 2020, 111045: https://doi.org/10.1016/j.msec.2020.111045

Application Note

Microscopic Characterization of Polymer Fibers with Mechanical Properties Similar to Dragline Spider Silk

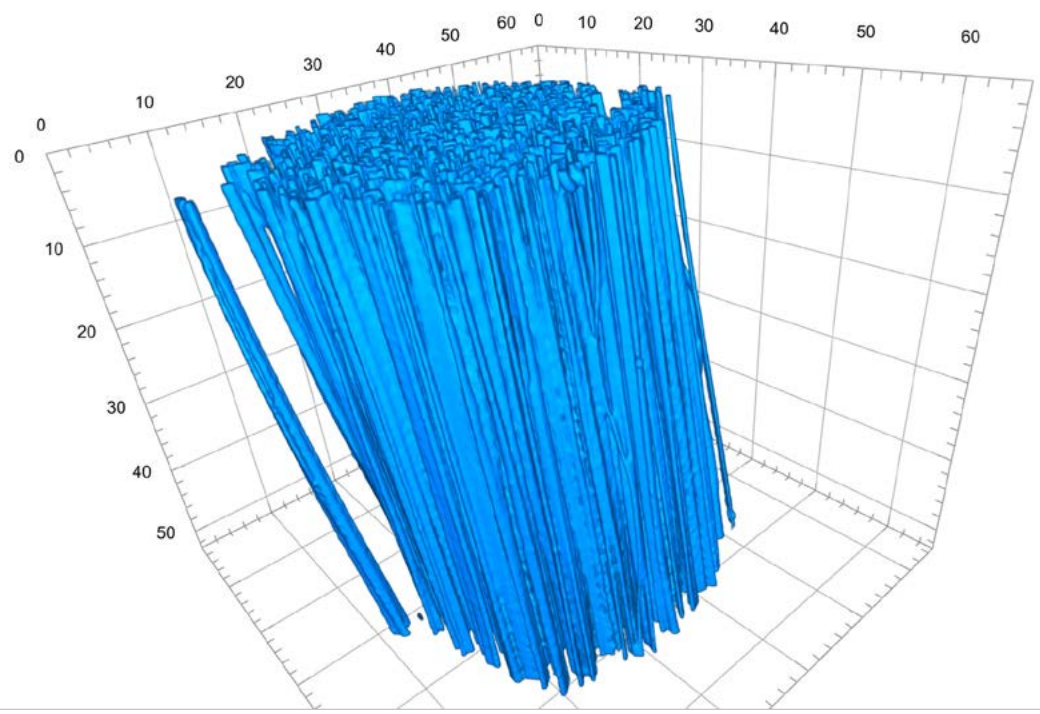

ZEISS

Seeing beyond

Authors: Juliana Martins de Souza e Silva, Ralf Wehrspohn
Microstructure-based Materials Design – mikroMD, Martin-Luther University Halle-Wittenberg, Germany
Xiaojian Liao, Seema Agarwal, Andreas Greiner
Macromolecular Chemistry and Bavarian Polymer Institute, University of Bayreuth, Bayreuth, Germany
Mohsen Samadi Khoshkhoo, Fang Zhou
Carl Zeiss Microscopy GmbH, Oberkochen, Germany
Date: July 2020

Introduction

Spider dragline silk has remarkable mechanical properties. It is highly stronger and tougher than steel on an equal weight basis, however, lighter, thinner and more flexible than steel. If it were possible to harvest spider silk commercially it could have been used for high-tech, commercial and consumer applications, such as bridge cables, aerospace components, biodegradable water bottles or antimicrobial medical devices based on its exceptional, superior properties. However, today there is no known way to produce spider silk in commercial quantities, because spiders are cannibalistic, they cannot be raised in concentrated colonies to produce silk. Furthermore, dragline spider silk is also known for its unique combination of strength and toughness. But this combination has been hard to replicate in synthetic fibers, since there is an intrinsic conflict between high strength and high toughness in materials science. As shown in the Table 1, dragline spider silk is even tougher than Kevlar®, which is currently one of the strongest polymer materials known.

	Material Toughness [J/g]	Tensile Strength [MPa]	Density [g/cm³]
Dragline spider silk	120-160	1,100-2,900	1,18-1,36
Kevlar®	30-50	2,600-4,100	1,44
Steel	2-6	300-2,000	7,84

Table 1. *Comparison of the properties of natural spider silk, Kevlar® and steel*

To push the limits of what is possible, scientists are trying to find a way to produce synthetic materials with a strength and toughness comparable to that of spider silk by designing an innovative microstructure of synthetic fibers. Therefore, microscopic characterization of such microstructure using SEM and XRM is necessary to understand the link of microstructure, process and property. In this application note, microscopic characterization of the synthetic fibers using ZEISS FESEM and XRM is introduced which helps to optimize the manufacturing process of such synthetic strong and tough polymer fibers. .

Polymer Fiber – Stronger and Tougher than Steel

Recently Liao et al. [1] successfully developed a new type of polymer fibers composed of multi-fibrillar polyacrylonitrile yarn with a toughness of 137 ± 21 J/g in combination with a tensile strength of 1236 ± 40 MPa. The nearly perfect uniaxial orientation of the fibrils by heat stretching, annealing under tension in the presence of linking molecules, is essential for the yarn's notable mechanical properties. This underlying principle can be used to create similar strong and tough fibers from other commodity polymers in the future and could be used in a variety of applications in areas such as biomedicine, satellite technology, textiles, aircrafts, and automobiles [1].

Microscopic Characterization of Polymer Fiber

As reported in [1] the stretched electro spun yarn was annealed at certain temperatures under tension, which leads to overall properties comparable to those of spider silk. Microscopic characterization shows that the small fibers are quite well aligned and cross-linked together via interconnecting molecules after an optimized annealing and tension process. Both electron and X-ray microscopy are used to characterize the morphology of the novel polymer fibers.

As shown in the SEM pictures taken using ZEISS FESEM (LEO 1530), the as-spun yarn has an average diameter of 130± 12 µm and consisted of ~3000 non-oriented individual fibrils with 1.17 ± 0.12 µm diameter before annealing and stretching processes (Fig.1 (A), (B)). Heat stretching of the yarns for several minutes results in their manifold elongation accompanied by a change in the macroscopic appearance (Fig.2 (A)) and the alignment of the fibrils in the yarns (Fig.2 (B)).

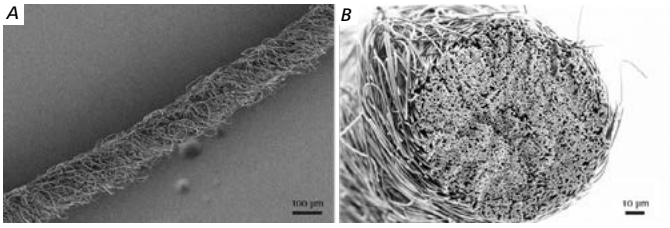

Fig. 1 *(A) SEM image of the long axis of the as-spun yarns before the annealing and stretching process. (B) SEM image of a cross-section of the as-spun yarns shown in Fig. 1 (A).*

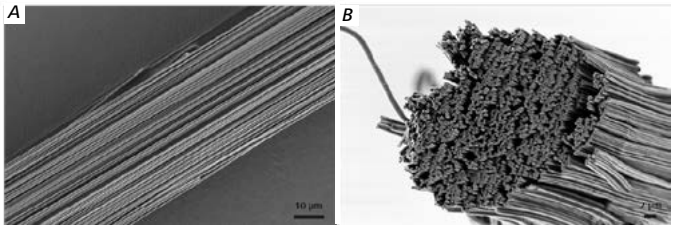

Fig. 2 *(A) SEM image of the long axis of stretched (at the stretch ratio of 8 and 160°C) and annealed (130°C for 4 hours) yarns. (B) SEM image of a cross-section of the stretched (at the stretch ratio of 8 and 160°C) and annealed (130°C for 4 hours) yarns.*

3D X-ray imaging [2] by means of ZEISS Xradia Ultra 810 X-ray microscope reveals the uniform orientation of the fibrils and enables the precise measurements of the diameters of single fibril as well as stretched and unstretched yarns. The tortuosity estimation, calculated using the 3D images, is equal to 1.00 for stretched yarns (at the stretch ratio of 8 and 160°C) and agrees well with the uniform orientation of the fibrils [1]. Fig. 3 shows a volumetric reconstruction of a section of a yarn. Fig. 4 shows one fibril from one yarn and Fig.5 a closer look inside of a yarn [2].

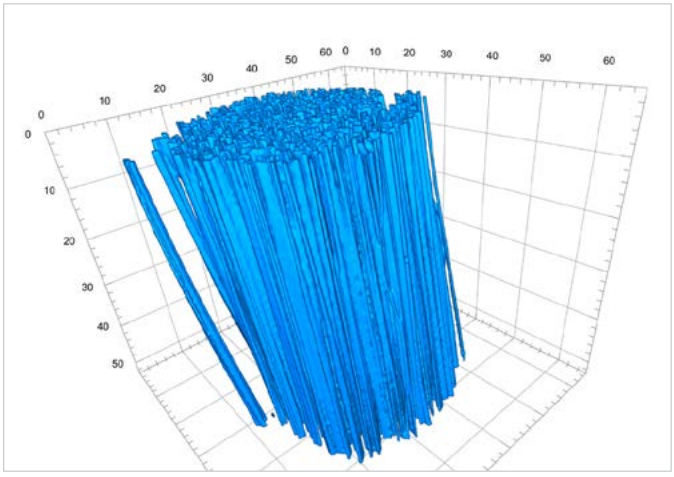

Fig. 3 *X-ray microscopy volumetric rendering of a section of a yarn*

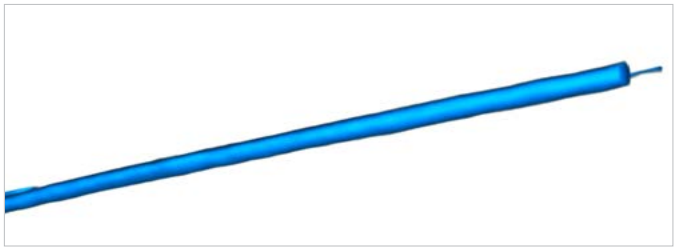

Fig. 4 *A single fibril of a yarn*

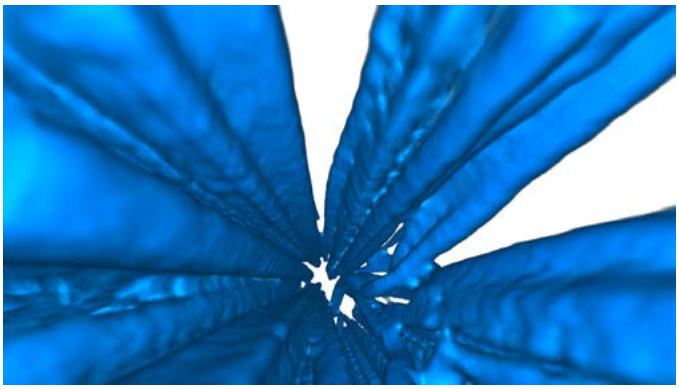

Fig. 5 *A closer look at inside of a yarn*

Conclusion

The ZEISS FESEM LEO 1530 is based on the proven Gemini technology with very high resolution and highest sample flexibility in surface sensitive imaging and analysis. It delivers unique contrast and is very suitable for beam sensitive samples like polymers, just because of its unique low-kV imaging performance.

ZEISS Xradia Ultra is a laboratory-based nanoscale 3D X-ray microscope (XRM) which enables non-destructive 3D or 4D tomography with a resolution in the sub-micrometer range for polymer samples. ZEISS Xradia Ultra delivers uniquely strong phase contrast using a Zernike-type phase plate to enhance the high-resolution imaging of low Z materials, such as polymers. The unique phase contrast approach has enabled the characterization of the nanostructure of the synthetic polymer fibers in this work.

Both a ZEISS FESEM and XRM were successfully applied to characterize the morphology and to understand the effects of the annealing and stretching process in order to optimize the overall properties of polymer fibers. Various samples such as protein fibers, porous materials, catalysts and drugs, and so on can be characterized using these microscopic methods to visualize 3D microstructures of samples and to estimate structural parameters using software analyses.

References

[1] X.J. Liao, et al. Science 2019, Vol. 366, Issue 6471, pp. 1376-1379, DOI: 10.1126/ science.aay9033
[2] ZEISS Blog: https://blogs.zeiss.com/microscopy/en/x-ray-microscopy-for-novel-polymeric-materials

Imprint

Boschstr. 12,
69469 Weinheim,
Germany
Email: info@wiley-vch.de

Editors:
Dr. Christene Smith &
Róisín Murtagh